Understanding the amplitudes of noise correlation measurements

Victor C. Tsai[1]

Received 23 April 2011; revised 17 June 2011; accepted 29 June 2011; published 24 September 2011.

[1] Cross correlation of ambient seismic noise is known to result in time series from which station-station travel-time measurements can be made. Part of the reason that these cross-correlation travel-time measurements are reliable is that there exists a theoretical framework that quantifies how these travel times depend on the features of the ambient noise. However, corresponding theoretical results do not currently exist to describe how the amplitudes of the cross correlation depend on such features. For example, currently it is not possible to take a given distribution of noise sources and calculate the cross correlation amplitudes one would expect from such a distribution. Here, we provide a ray-theoretical framework for calculating cross correlations. This framework differs from previous work in that it explicitly accounts for attenuation as well as the spatial distribution of sources and therefore can address the issue of quantifying amplitudes in noise correlation measurements. After introducing the general framework, we apply it to two specific problems. First, we show that we can quantify the amplitudes of coherency measurements, and find that the decay of coherency with station-station spacing depends crucially on the distribution of noise sources. We suggest that researchers interested in performing attenuation measurements from noise coherency should first determine how the dominant sources of noise are distributed. Second, we show that we can quantify the signal-to-noise ratio of noise correlations more precisely than previous work, and that these signal-to-noise ratios can be estimated for given situations prior to the deployment of seismometers. It is expected that there are applications of the theoretical framework beyond the two specific cases considered, but these applications await future work.

Citation: Tsai, V. C. (2011), Understanding the amplitudes of noise correlation measurements, *J. Geophys. Res.*, *116*, B09311, doi:10.1029/2011JB008483.

1. Introduction

[2] *Shapiro and Campillo* [2004] first showed that traveltime measurements obtained through cross correlation of ambient seismic noise resemble those from more traditional source-station measurements. Since then, the field of ambient noise correlation has exploded, with many authors focusing on traveltime tomography [e.g., *Shapiro et al.*, 2005; *Sabra et al.*, 2005a; *Yao et al.*, 2006; *Cho et al.*, 2007; *Lin et al.*, 2008], and others focusing on temporal changes in traveltimes [e.g., *Brenguier et al.*, 2008; *Meier et al.*, 2010]. It is now also well recognized that these noise correlation traveltimes depend on the noise source distribution in a predictable way [e.g., *Lin et al.*, 2008; *Tsai*, 2009; *Yao and van der Hilst*, 2009; *Harmon et al.*, 2010; *Tromp et al.*, 2010], and that performing a joint inversion for structure and noise distribution can account for the (typically small) biases that would result from assuming a uniform noise distribution [e.g., *Yao and van der Hilst*, 2009].

[3] Recently, researchers have begun to be interested in going beyond traveltime measurements and using the amplitudes of the noise correlations. For example, *Prieto and Beroza* [2008] have used noise correlation amplitudes to infer ground motions and *Prieto et al.* [2009] have used coherency amplitudes to infer attenuation between station pairs (in the period range 5–20 s). Despite the general success of these studies at producing reasonable values of inferred parameters, there remains some question as to how accurate their measurements are. While traveltime measurements are understood theoretically as described above, amplitude measurements do not have a corresponding theoretical background, except when noise is equipartitioned [*Snieder*, 2007; *Larose et al.*, 2007] (a very specific case which is not satisfied by ambient seismic noise on the Earth). A few numerical experiments have been performed that show how amplitudes are affected in very particular cases [*Cupillard and Capdeville*, 2010], but no general theoretical framework exists. For this reason, it is currently not possible to quantify the accuracy of noise studies that rely on amplitudes. To address this gap in the literature, we provide a ray-theoretical framework for understanding the amplitudes of noise correlation measurements and how these amplitudes depend on the noise source distribution (section 2). Using these results, we then show that the way in which coherency amplitudes decay with station-station distance depends on the noise source distribution in a significant way (section 3.1).

[1]Seismological Laboratory, California Institute of Technology, Pasadena, California, USA.

0148-0227/11/2011JB008483

[4] In addition to providing a theory to understand how to interpret the amplitudes of coherency measurements, this framework also allows us to calculate how large the coherent 'signals' are compared to the 'noise' level produced by incoherent signals. Having a high 'signal-to-noise' ratio, *SNR*, in noise correlations is the first requirement on obtaining a robust measurement from noise correlation techniques. Knowledge of this *SNR* is therefore potentially useful to researchers interested in applying noise correlation techniques in exotic locations or in other places that are not well characterized. We show that we can estimate the *SNR* using a small number of parameters that may be approximately known, and therefore be able to determine the likelihood of obtaining a robust signal in certain situations prior to deploying seismometers (section 3.2).

2. Derivations for Noise Correlation

[5] In this study, we follow the approach of *Tsai* [2009] to quantify cross-correlation amplitudes. In this approach, it is assumed that there exists a spatial distribution of noise sources and that the response at each station can be described by an integral over these sources. Here, we assume a uniform velocity medium and concentrate on understanding the role of the noise source distribution on the cross correlation amplitudes. It is expected that velocity heterogeneities have effects similar to those previously documented [*Tsai*, 2009]. In our previous studies, only traveltime measurements were calculated and it was therefore not necessary to explicitly consider the effects of attenuation. In order to properly account for attenuation, we now base our discussion on the damped wave equation

$$\frac{1}{c^2}\frac{\partial^2 u}{\partial t^2}+\frac{2\alpha}{c}\frac{\partial u}{\partial t}=\nabla^2 u, \tag{1}$$

where t is time, c is phase velocity and α is an attenuation coefficient. In principle, u expresses any single mode displacement component (e.g., P, S, Rayleigh or Love), with c and α interpreted accordingly. Performing a Fourier decomposition (with time dependence $e^{-i\omega t}$, where ω is frequency) for the two-dimensional (2D) damped wave equation and allowing for potentially frequency-dependent $c \equiv c(\omega)$ and $\alpha \equiv \alpha(\omega)$, one can compute the Green's function as

$$G(\boldsymbol{x},\omega;\boldsymbol{s}) = \frac{i}{4}H_0^{(1)}\left(\frac{\omega r}{c}\sqrt{1+\frac{2i\alpha c}{\omega}}\right) \approx \frac{i}{4}e^{-\alpha r}H_0^{(1)}\left(\frac{\omega r}{c}\right), \tag{2}$$

where $H_k^{(1)}$ is a Hankel function of the first kind, $r \equiv r(\boldsymbol{s},\boldsymbol{x})$ is the distance from the source ($\boldsymbol{s}$) to the receiver ($\boldsymbol{x}$), and the approximation holds as long as attenuation is weak ($\alpha \ll \omega/c$). We note that this 2D Green's function should apply to (2D) surface waves, which will be the main focus of this study.

[6] Similar expressions for the 1D and 3D versions of the damped wave equation can easily be obtained. In fact, asymptotically (for $\omega r/c \gg 1$), all three scaled Green's functions can be written in the time domain (for a single-frequency wave and arbitrary non-unit amplitude) as

$$\begin{aligned} G(\boldsymbol{x},t;\boldsymbol{s}) &= A(\boldsymbol{s})\, e^{-\alpha r} r^{-(D-1)/2} \cos\left[\omega\left(t-\frac{r}{c}\right)+\phi\right] \\ &= A(\boldsymbol{s})\, \epsilon(r)\, \cos\left[\omega\left(t-\frac{r}{c}\right)+\phi\right], \end{aligned} \tag{3}$$

where A is a source amplitude factor, ϕ is a phase factor, D is the dimensionality (either 1, 2, or 3), and we introduce $\epsilon(r) \equiv e^{-\alpha r}/r^{(D-1)/2}$. At this point, we observe that an approximate ray-theory solution can also be given for a medium in which the velocity is smoothly varying, where r is reinterpreted as the raypath length from source to receiver, $1/c$ is the mean phase slowness along this path, and α can be related to the path-averaged quality factor Q by $\alpha = \omega/(2UQ)$, where U is group velocity [*Mitchell*, 1995]. Equation (3) ignores any site amplification or focusing effects; site amplification could be accounted for by including an extra term $S(\boldsymbol{x})$ multiplying the right-hand-side of equation (3).

[7] For a discrete set of noise sources, the total displacement response is given simply by a sum over these different sources. On the other hand, for a continuous distribution of noise, we can treat the source amplitude $A(\boldsymbol{s})$ as source density (e.g., amplitude per unit surface area or per unit volume). In the case of equation (2) (with source amplitude $4A$), then the total displacement response is given by

$$\begin{aligned} u(\boldsymbol{x},t) &= \Re\left[\int 4A(\boldsymbol{s})\, G(\boldsymbol{x},\omega;\boldsymbol{s})\, e^{-i\omega t} d\boldsymbol{s}\right] \\ &= \int \frac{A(\boldsymbol{s})}{e^{\alpha r}}\left[J_0\left(\frac{\omega r}{c}\right)\sin(\omega t+\phi) - Y_0\left(\frac{\omega r}{c}\right)\cos(\omega t+\phi)\right] d\boldsymbol{s}, \end{aligned} \tag{4}$$

where $\Re[z]$ denotes the real part of z, and J_k and Y_k are Bessel functions (of order k) of the first and second kind, respectively. Alternatively, in the case of equation (3) (with source amplitude A as given), the response is given by

$$\begin{aligned} u(\boldsymbol{x},t) &= \int G(\boldsymbol{x},t;\boldsymbol{s})\, d\boldsymbol{s} \\ &= \int A(\boldsymbol{s})\epsilon(r)\, \cos\left[\omega\left(t-\frac{r}{c}\right)+\phi\right] d\boldsymbol{s}. \end{aligned} \tag{5}$$

[8] So far, the entire displacement field has been assumed to be a sum of sources described by either equation (2) or equation (3). However, there exist non-wave sources of seismic displacement, including local seismograph housing effects, electromagnetic effects, and other anelastic effects [e.g., *Tsai et al.*, 2004; *Berger et al.*, 2004; *Zurn et al.*, 2007]. These noise sources are only seen locally and do not propagate to other stations and are therefore sources of incoherent energy. Thus, added to either equation (4) or equation (5) is a term $A_{Ix}\cos(\omega t + \phi_{Ix})$ where A_{Ix} is the incoherent noise amplitude and ϕ_{Ix} is the incoherent noise phase at the location $\boldsymbol{x}$. Equation (4) is therefore modified to be

$$u(\boldsymbol{x},t) = \Re\left[\int 4A(\boldsymbol{s})\, G(\boldsymbol{x},\omega;\boldsymbol{s})\, e^{-i\omega t} d\boldsymbol{s}\right] + A_{Ix}\cos(\omega t+\phi_{Ix}), \tag{6}$$

and equation (5) is modified to be

$$u(\boldsymbol{x},t) = \int G(\boldsymbol{x},t;\boldsymbol{s})\, d\boldsymbol{s} + A_{Ix}\cos(\omega t+\phi_{Ix}). \tag{7}$$

It should be noted that the incoherent term only includes sources that do not propagate elastically. All sources that

propagate elastically are included in the coherent term even when the effect of these sources attenuates rapidly.

[9] Finally, as in the work of *Tsai* [2010], we define the normalized cross correlation as

$$C_{xy}^{T}(t) \equiv \frac{1}{2T}\int_{-T}^{T} u(\boldsymbol{x},\tau)\, u(\boldsymbol{y},\tau+t)\, d\tau, \tag{8}$$

the limiting value as

$$C_{xy}(t) \equiv \lim_{T\to\infty} C_{xy}^{T}(t), \tag{9}$$

and the ensemble cross correlation as

$$C_{xyM}^{E}(t) \equiv \frac{1}{M}\sum_{i=1}^{M} {}_{i}C_{xy}^{T}(t), \tag{10}$$

where each ${}_{i}C_{xy}^{T}(t)$ is a different realization (i.e. the ϕ are random). As discussed by *Tsai* [2010], if the physical system in which noise is generated is naturally attenuating, and has a quality factor Q_P, then an approximation for M in terms of Q_P and the total correlation time T_0 is $M \approx \omega T_0/Q_P = T_0/T_a$, where $T_a \equiv Q_P/\omega$ is an e-folding attenuation time for the system. (Alternatively, Q_P can be defined in terms of T_a.) We note that this definition of cross correlation does not have additional normalization that accounts explicitly for the total energy observed (see section 3.1). We also note that if A changes slowly in time, all of the equations described above remain unchanged, with the recognition that it is a time-averaged A that should be used [e.g., *Tsai*, 2009]. Furthermore, any preprocessing of data such as temporal normalization can be understood to just modify the time averaging used to determine A.

[10] Substituting equation (6) or equation (7) into equation (10) gives the most general expression for the narrowband cross correlation under the assumptions stated above. *Tsai* [2010] observed that as long as attenuation is relatively weak and correlation times are long, then one can use the expressions for calculating equation (9) in place of those for equation (8). In this case, it was also previously shown that expressions for $C_{xy}(t)$ simplify considerably. In particular, the correlation of two cosine signals is a cosine with phase equal to the difference in phases of the original signals. For the remainder of this work, we shall assume, as in previous work, that these properties hold for all correlations performed. As also discussed by *Tsai* [2010], common processing techniques cause leakage of energy from neighboring frequencies so that the measured narrowband cross correlation is actually affected by sources within a small (but non-negligible) range of frequencies.

[11] Unless otherwise stated, from this point onwards, only the 2D (surface wave) case will be considered, and the approximate version of equation (7) (with $D = 2$) will be used instead of the exact version of equation (6) because it is much more amenable to analytic simplification. Since equation (2) approaches equation (3) asymptotically, equation (7) will only accrue errors when r is not in the far-field. Furthermore, as will be shown in section 3.1.5, this error is typically relatively minor, even when r is relatively small. Since the primary purpose of this current work is to show the approximate form of amplitudes for various source distributions, and it is not to precisely model any particular source distribution, this error can be tolerated. We note that if precise values were desired, numerical evaluation of equation (6) could be performed (again, see section 3.1.5).

2.1. One Source With Incoherent Noise

[12] For simplicity, we first consider the case of 1 discrete noise source (at location $\boldsymbol{s}_1$ anywhere) with incoherent noise so that equation (7) gives

$${}_{i}u(\boldsymbol{x},t) = A_1\epsilon(r_{1x})\,\cos\left[\omega\left(t-\frac{r_{1x}}{c}\right)+\phi_i\right] + A_{Ix}\cos[\omega t+\phi_{Ixi}], \tag{11}$$

where ${}_{i}u(\boldsymbol{x}, t)$ is the displacement in the ith realization, $A_j \equiv A(\boldsymbol{s}_j)$, $r_{jx} \equiv r(\boldsymbol{s}_j, \boldsymbol{x})$, and ϕ_i is the phase of the noise source in the ith realization. Note that we define a noise source as having a constant amplitude but varying phase through different realizations. Making use of the simplifications of *Tsai* [2010] results in

$$\begin{aligned} 2C_{xyM}^{E} = {} & A_1^2\epsilon(r_{1x})\,\epsilon(r_{1y})\,\cos\left[\omega\left(t-\frac{r_{1y}-r_{1x}}{c}\right)\right] \\ & + \frac{A_1A_{Iy}}{\sqrt{M}}\epsilon(r_{1x})\,\cos\left[\omega t+\phi_1^{av}\right] \\ & + \frac{A_1A_{Ix}}{\sqrt{M}}\epsilon(r_{1y})\,\cos\left[\omega t+\phi_2^{av}\right] \\ & + \frac{A_{Ix}A_{Iy}}{\sqrt{M}}\cos\left[\omega t+\phi_3^{av}\right], \end{aligned} \tag{12}$$

where ϕ_k^{av} is the average phase difference of the M realizations.

[13] This 1-source form of the cross correlation is not particularly useful by itself but later results will have similar characteristics that are more easily understood in the 1-source expression. For now, we simply note that the first term of equation (12) represents the 'signal' term and that the other 3 terms are "noise" terms that are not desired. Since $\sqrt{M} = \sqrt{T_0/T_a}$ grows as the total correlation time (T_0) increases, we observe that the signal-to-noise ratio grows with time.

2.2. Two Independent Sources

[14] Next, we consider the case of 2 independent discrete noise sources (at locations $\boldsymbol{s}_1$ and $\boldsymbol{s}_2$), without any incoherent sources (for simplicity), so that

$$\begin{aligned} {}_{i}u(\boldsymbol{x},t) = {} & A_1\epsilon(r_{1x})\,\cos\left[\omega\left(t-\frac{r_{1x}}{c}\right)+\phi_{1i}\right] \\ & + A_2\epsilon(r_{2x})\,\cos\left[\omega\left(t-\frac{r_{2x}}{c}\right)+\phi_{2i}\right]. \end{aligned} \tag{13}$$

Again making use of the simplifications of *Tsai* [2010] results in

$$\begin{aligned} 2C_{xyM}^{E} = {} & A_1^2\epsilon(r_{1x})\,\epsilon(r_{1y})\,\cos\left[\omega\left(t-\frac{r_{1y}-r_{1x}}{c}\right)\right] \\ & + A_2^2\epsilon(r_{2x})\,\epsilon(r_{2y})\,\cos\left[\omega\left(t-\frac{r_{2y}-r_{2x}}{c}\right)\right] \\ & + \frac{A_1A_2}{\sqrt{M}}\left\{\epsilon(r_{1y})\,\epsilon(r_{2x})\,\cos\left[\omega\left(t-\frac{r_{1y}-r_{2x}}{c}\right)+\phi_1^{av}\right]\right. \\ & \left. + \epsilon(r_{2y})\,\epsilon(r_{1x})\,\cos\left[\omega\left(t-\frac{r_{2y}-r_{1x}}{c}\right)+\phi_2^{av}\right]\right\}. \end{aligned} \tag{14}$$

We note that $\epsilon(r_{sx})\epsilon(r_{sy}) = e^{-\alpha(r_{sx}+r_{sy})}/\sqrt{r_{sx}r_{sy}}$ (for $D = 2$).

[15] This very limited 2-source form of the cross correlation is already useful because it roughly approximates the high-frequency surface-wave limit in which the dominant noise sources are at the 2 stationary phase points [*Snieder*, 2004]. Without performing an integral over the actual distribution of noise sources, this 2-source approximation does not contain the $\pi/4$ phase shift (in 2D), e.g., as discussed by *Tsai* [2009], and also does not provide the true amplitude of the sources at the 2 points, but otherwise is a reasonable approximation (see section 2.4). One interesting point to observe is that equation (14) has attenuation terms proportional to $e^{-\alpha(r_{sx}+r_{sy})}$. Thus, the attenuations are added together, and not subtracted as might be expected from Green's function relationships that hold when sources are distributed uniformly, e.g., as in the work of *Snieder* [2007].

2.3. Two Related Sources

[16] In section 2.2, it was assumed that the 2 noise sources were independent of each other. However, in general, certain subsets of noise sources can be dependent. For example, noise sources that are close to each other are often excited by the same physical processes (e.g. ocean waves) such that the signals generated are in phase with each other rather than being independent. Similarly, if there is a strong scatterer, the phase of the source at the scatterer is determined by the phase of the primary sources plus the extra time delay associated with the scattering path. For either of these situations, we can modify equation (13) to account for the dependence so that

$$
\begin{aligned}
{}_iu(\boldsymbol{x},t) \;&= A_1\epsilon(r_{1x})\;\cos\left[\omega\left(t-\frac{r_{1x}}{c}\right)+\phi_{1i}\right]\\
&\quad + A_2\epsilon(r_{2x})\;\cos\left[\omega\left(t-\frac{r_{2x}}{c}-\Delta t\right)+\phi_{1i}\right],
\end{aligned}
\tag{15}
$$

where Δt is the time delay of the source at $\boldsymbol{s}_2$ relative to the source at $\boldsymbol{s}_1$. It should be noted that Δt is a total time delay that includes all potential sources of time lag, including path and scattering effects.

[17] Performing the same analysis with equation (15) yields

$$
\begin{aligned}
2C^E_{xyM} = {}& A_1^2\epsilon(r_{1x})\;\epsilon\left(r_{1y}\right)\;\cos\left[\omega\left(t-\frac{r_{1y}-r_{1x}}{c}\right)\right]\\
&+ A_1A_2\epsilon(r_{1x})\;\epsilon\left(r_{2y}\right)\;\cos\left[\omega\left(t-\frac{r_{2y}-r_{1x}}{c}-\Delta t\right)\right]\\
&+ A_1A_2\epsilon\left(r_{1y}\right)\;\epsilon(r_{2x})\;\cos\left[\omega\left(t-\frac{r_{1y}-r_{2x}}{c}+\Delta t\right)\right]\\
&+ A_2^2\epsilon(r_{2x})\;\epsilon\left(r_{2y}\right)\;\cos\left[\omega\left(t-\frac{r_{2y}-r_{2x}}{c}\right)\right].
\end{aligned}
\tag{16}
$$

When $\boldsymbol{s}_1 \approx \boldsymbol{s}_2$ (so that $r_{1x} \approx r_{2x}$ and $\Delta t \approx 0$) then equation (16) simplifies to

$$
2C^E_{xyM} = \;(A_1+A_2)^2\epsilon(r_{1x})\;\epsilon\left(r_{1y}\right)\;\cos\left[\omega\left(t-\frac{r_{1y}-r_{1x}}{c}\right)\right]. \tag{17}
$$

This simplified form of equation (16) will be used in later sections to describe dependent noise sources with approximately the same source region. It should be noted that both equations (16) and (17) differ from equations (12) and (14) in that there is no decay of cross terms with $\sqrt{M}$.

2.4. General Continuous Distribution

[18] With equations (12), (14) and (16) describing all of the pairwise correlation possibilities, it is now relatively straightforward to generalize to an arbitrary distribution of noise sources. However, one must correctly account for the various dependencies of the different sources. To simplify the analysis, here, we make a few different assumptions. First, we assume that non-overlapping regions can be defined for which sources are dependent within each region but independent between regions. With this assumption, the integral in equation (5) can be broken into a sum over the N discrete regions, each of which has related sources (as described in section 2.3). This assumption is not valid for the reflection problem (see Appendix A) but is a reasonable approximation for primary sources. Second, we assume that each of these regions can be described with one effective amplitude and cross-correlation time delay. This can be done by performing the integral in equation (5) separately for each of the N regions and using the generalization of equation (16) to solve for a region-averaged A_j and r_{jx}. With these assumptions, applying equations (12), (14) and (16) pairwise results in

$$
\begin{aligned}
2C^E_{xyM} = {}& \sum_{j=1}^{N} A_j^2\epsilon\left(r_{jx}\right)\;\epsilon\left(r_{jy}\right)\;\cos\left[\omega\left(t-\frac{r_{jy}-r_{jx}}{c}\right)\right]\\
&+ \frac{1}{\sqrt{M}}\sum_{j=1}^{N}\sum_{k\neq j} A_jA_k\epsilon\left(r_{jx}\right)\;\epsilon\left(r_{ky}\right)\;\cos\left[\omega t+\phi^{av}_{jk}\right]\\
&+ \frac{A_{Iy}}{\sqrt{M}}\sum_{j=1}^{N} A_j\epsilon\left(r_{jx}\right)\;\cos\left[\omega t+\phi^{av}_{j}\right]\\
&+ \frac{A_{Ix}}{\sqrt{M}}\sum_{j=1}^{N} A_j\epsilon\left(r_{jy}\right)\;\cos\left[\omega t+\phi^{av}_{j}\right]\\
&+ \frac{A_{Ix}A_{Iy}}{\sqrt{M}}\cos[\omega t+\phi^{av}],
\end{aligned}
\tag{18}
$$

where the ϕ^{av} are random. The first 2 terms arise from applying equation (14), the last 3 terms arise from applying equation (12), and equation (16) is used to calculate the region-averaged A_j and r_{jx}.

[19] It is useful to note that in equation (18), the first term represents all coherent arrivals and that the second term has many more elements ($N^2 - N \approx N^2$) compared to all of the other incoherent terms (N elements in the third and fourth terms and only 1 element in the fifth term). Thus, in order for the third term to be larger than the second term, one must have $A_{Iy} > NA_{av}\epsilon(r_y^{av})$, where $A_{av}\epsilon(r_y^{av})$ is the average value of $A_j\epsilon(r_{jy})$; similarly, one must have $A_{Ix} > NA_{av}\epsilon(r_x^{av})$ for the fourth term to be larger than the second; and both conditions must hold for the fifth term to dominate the incoherent signal. For much of this work, it will be assumed that neither condition holds, and that the main incoherent signal is from 'realization noise', the second term of equation (18). (In section 3.2.5, however, we show that this assumption may not always be valid.) For this case, equation (18) simplifies to

$$
\begin{aligned}
2C^E_{xyM} \approx {}& \sum_{j=1}^{N} A_j^2\epsilon\left(r_{jx}\right)\;\epsilon\left(r_{jy}\right)\;\cos\left[\omega\left(t-\frac{r_{jy}-r_{jx}}{c}\right)\right]\\
&+ \frac{N}{\sqrt{M}}\overline{A}^2\,\epsilon\left(\bar{r}_x\right)\;\epsilon\left(\bar{r}_y\right)\;\cos[\omega t+\phi^{av}],
\end{aligned}
\tag{19}
$$

where $\overline{A}^2$ is a weighted average value of A_jA_k and $\bar{r}_x$ is a weighted average value of r_{jx} (weighted by ϵ such that $\overline{A}^2\epsilon(\bar{r}_x)\epsilon(\bar{r}_y)$ is the root mean square average of $A_jA_k\epsilon(r_{jx})\epsilon(r_{ky})$).

In this simplification, we have used the fact that a random walk (from random ϕ_{jk}^{av}) of N^2 unit steps in the complex plane results in a total distance traveled of N units.

[20] If each of the N regions discussed above is relatively small, then one can further simplify equation (19) so that its first term is approximated as a spatial integral over the entire source region instead of a sum, resulting in

$$2C_{xyM}^{E} \approx \int_{\boldsymbol{s}} A_s^2 \epsilon(r_{sx})\ \epsilon(r_{sy})\ \cos\left[\omega\left(t - \frac{r_{sy} - r_{sx}}{c}\right)\right]\ d\boldsymbol{s} + \frac{N}{\sqrt{M}} \overline{A}^2 \epsilon(\overline{r}_x)\ \epsilon(\overline{r}_y) \cos[\omega t + \phi^{av}], \tag{20}$$

where now A_s is a source density, as in equation (4), rather than a source amplitude, as in equation (19). Similarly, $\overline{A}^2\epsilon(\overline{r}_x)\epsilon(\overline{r}_y)$ is now a root mean square average calculated by integration rather than summation.

3. Application to Coherency and Signal-to-Noise Ratios

[21] The results derived in section 2 have applicability to at least two separate issues of interest. The first issue that we discuss relates to how attenuation measurements can be made from noise correlation studies. Previous studies, starting with *Prieto et al.* [2009], have used noise correlation measurements to infer attenuation parameters (e.g. α as a function of ω) by assuming the amplitudes of the observed noise correlations depend on these parameters in a specific way. In section 3.1, we show that this dependence can be very different from the assumed one for certain distributions of noise. In fact, only when sources are distributed uniformly everywhere (in the 2D plane) is the assumption valid. In all other cases examined, the dependence on attenuation parameters is different from that of *Prieto et al.* [2009].

[22] The second issue that we address is whether we can understand how large the noise correlation signal-to-noise ratio would be in a new situation of interest. The signal-to-noise ratio being relatively large is a prerequisite to obtaining a robust signal. Knowledge of this ratio is therefore potentially of interest to any researcher who wants to try noise correlation techniques in a new location or in a novel environment. In this case, it would be useful to know the plausibility of achieving a robust result prior to deploying a set of seismometers, an operation that can potentially be quite expensive. In section 3.2, we show that knowledge of a few key parameters allows for the calculation of the signal-to-noise ratio, and we show a few examples of this.

[23] We note that in both sections 3.1 and 3.2, we have made a number of simplifying assumptions, such as the spatial uniformity of α and c. The more general case is not conceptually more difficult and numerical results for the general case can easily be calculated with the same framework. However, we believe that the analytic expressions we derive and the ease with which one can observe the dependence on certain variables in these expressions to be more useful to the community than a host of numerical results (at least at this point in time). Therefore, we make no attempt to examine more complex cases.

3.1. Attenuation Measurements From Coherency

[24] *Prieto et al.* [2009] recently proposed a method for measuring attenuation using the coherency of noise. In this work, they assume that the observed coherency is equal to the theoretical coherency for uniform noise and no attenuation multiplied by an attenuation term equal to $e^{-\alpha\Delta x}$, where $\Delta x \equiv r_{xy}$ is the station-station spacing. In the framework described here, the observed coherency is given by

$$\hat{C}_{xyM}^{E}(\omega) \equiv \frac{C_{xyM}^{E}(\omega)}{\sqrt{C_{xxM}^{E}(\omega)\ C_{yyM}^{E}(\omega)}}. \tag{21}$$

When the 3 terms on the right-hand side of equation (21) have the same phase, the division can be done in the time domain; when the phases are different, the division must be done in the frequency domain (e.g., with the Fourier transform of $\cos[\omega_0 t - \phi]$ being $[\delta(\omega - \omega_0) + \delta(\omega + \omega_0)]\ e^{-i\phi}$, up to a normalization factor). The *Prieto et al.* [2009] method is then equivalent to assuming that

$$\Re\left[\hat{C}_{xyM}^{E}\right] = e^{-\alpha r_{xy}} J_0\left(\frac{\omega r_{xy}}{c}\right), \tag{22}$$

and this expression should hold for every choice of ω. (We note that *Aki* [1957] showed that in the absence of attenuation, an azimuthally averaged coherency is equal to $J_0(\omega r_{xy}/c)$.) Throughout this section, we take the limit $M \to \infty$ in all expressions, and therefore discuss only the coherent part of the cross correlation signal, $C_{xy}^{E} \equiv \lim_{M\to\infty} C_{xyM}^{E}$. For stations with large A_{Ix}, this is not a good approximation, and there will be additional biases that the expressions derived below do not express. Accounting for these dependencies is beyond the scope of this work.

[25] In the following sections, we consider five different noise distributions. These 5 distributions are chosen as relatively simple examples for which closed-form solutions can be determined. While true noise source distributions are unlikely to be precisely modeled with any of these 5 distributions (all of which have some form of axial symmetry), they provide a guideline for whether the *Prieto et al.* [2009] assumption is likely to be valid or if some alternative assumptions are likely to be better. We also note that 3 of the 5 distributions are chosen to be azimuthally uniform such that the known difficulties in having a non-azimuthally uniform source distribution can be separated from the effects of source distance. It will be seen that although the azimuthally uniform source distributions result in phases that are unbiased, the amplitudes can still decay differently than expected of equation (22). It may also be noted that if data is azimuthally averaged, as is done by *Prieto et al.* [2009], then the source distribution is effectively averaged azimuthally, and it would be most appropriate to compare results with these azimuthally uniform distributions.

[26] In each section, we first calculate the cross correlation C_{xy}^{E} and autocorrelation C_{xx}^{E} prior to calculating the coherency $\hat{C}_{xy}^{E}$. All of these results are summarized in Table 1. It is expected that these cross correlation and autocorrelation results may be useful beyond their use in determining coherency. As just one example of this, in section 3.1.6, we discuss how the results of the previous sections can be used to understand some of the numerical experiments of *Cupillard and Capdeville* [2010].

3.1.1. Uniform Distribution of Far-Field Surface Waves

[27] The simplest, yet somewhat realistic, distribution of noise sources is a uniform distribution of far-field surface-wave

Table 1. Summary of the Cross Correlation, Autocorrelation, Real Part of the Coherency and Signal-to-Noise Ratio, *SNR*, for the Different Scenarios Considered[a]

	$2C^E_{xy}(t)$	$2C^E_{xx}(t)$	$\Re[\hat{C}^E_{xy}(\omega)]$	*SNR*
One source	$A_1^2\epsilon(r_{1x})\epsilon(r_{1y})\cos\,\omega(t-\frac{r_{1y}-r_{1x}}{c})$	$A_1^2\epsilon(r_{1x})^2\,\cos(\omega t)$	$\cos[\frac{\omega(r_{1y}-r_{1x})}{c}]$	∞
Two sources				$\frac{A_1}{\sqrt{2}A_2}\sqrt{\frac{T_0}{T_a}}$
Uniform far-field	$\frac{A^2e^{-2\alpha R}}{R}\cos(\omega t)J_0\,(\frac{\omega r_{xy}}{c})$	$\frac{A^2e^{-2\alpha R}}{R}\cos(\omega t)I_0\,(\alpha r_{xy})$	$\frac{1}{I_0(\alpha r_{xy})}J_0(\frac{\omega r_{xy}}{c})$	$F\equiv\sqrt{\frac{2c}{\pi\omega r_{xy}}\frac{T_0}{T_a}}$
One-sided far-field	$\frac{A^2e^{-2\alpha R}}{R}\Re[e^{i\omega t}\cdot(J_0-iH_0)]$	$\frac{A^2e^{-2\alpha R}}{R}\cos(\omega t)[I_0-L_0]$	$\frac{J_0}{\sqrt{I_0^2-L_0^2}}$	F
Arbitrary far-field	$\frac{e^{-2\alpha R}}{R}\Re[e^{i\omega t}\Sigma_k(-i)^k a_k J_k]$	$\frac{e^{-2\alpha R}}{R}\cos(\omega t)\Sigma_k(-1)^k a_k I_k$	$\frac{\sum_k(-1)^k a_{2k}J_{2k}}{\sqrt{\sum_k a_k I_k}\sqrt{\sum_k(-1)^k a_k I_k}}$	$\frac{A_\theta^2}{\bar{A}^2}\cdot F$
Including near-field	$\frac{2A_\theta^2}{\alpha}e^{-\alpha r_{xy}}\cos(\omega t)J_0$	$\frac{2\bar{A}^2}{\alpha}\cos(\omega t)$	$\frac{A_\theta^2}{\bar{A}^2}e^{-\alpha r_{xy}}J_0$	$\frac{A_\theta^2}{\bar{A}^2}e^{-\alpha r_{xy}}\cdot F$
Near-field (only)	$2\pi A_\theta^2\cos(\omega t)J_0\sqrt{R^2-\frac{r_{xy}^2}{4}}$	$2\pi R\bar{A}^2\cos(\omega t)$	$\frac{A_\theta^2}{\bar{A}^2}\sqrt{1-\frac{r_{xy}^2}{4R^2}}\cdot J_0$	$\frac{A_\theta^2}{\bar{A}^2}\sqrt{1-\frac{r_{xy}^2}{4R^2}}\cdot F$
Reflection		$\Gamma A_1^2\epsilon^2(r_{1x})\,\cos[\omega(t-\Delta t)]$		$\frac{\Gamma A_1^{*2}}{(A_1^*+A_2^*)^2}\sqrt{\frac{T_0}{T_a}}$

[a]When not written explicitly, J_k and H_0 are functions of $\omega r_{xy}/c$ and I_k and L_0 are functions of αr_{xy}. In this table, *SNR* is for the case without incoherent terms (A_{Ix}) and F is the *SNR* for the uniform far-field case. See text for how *SNR* depends on A_{Ix}.

noise sources. For example, if ocean microseisms are the primary source of noise, as may be expected for many continental seismic stations [*McNamara and Buland*, 2004], and the distance to the ocean is far relative to the station-station distance, then this distribution may be appropriate. In this case, $A_s = A$ is constant along a large circle (with radius $R \gg r_{xy}$) centered halfway between the two stations and A_s is zero elsewhere (see Figure 1a). For this simple case, $r_{sy} = R + \cos\theta \cdot r_{xy}/2$, $r_{sx} = R - \cos\theta \cdot r_{xy}/2$, and $r_{sy} - r_{sx} = r_{xy}\cos\theta$, where θ is the azimuth of the source relative to the station-station line. Using these expressions, we can simplify equation (20) to be

$$\begin{aligned}2C^E_{xy} &\approx \frac{A^2}{2\pi}\int_0^{2\pi}\frac{e^{-\alpha(r_{sx}+r_{sy})}}{\sqrt{r_{sx}r_{sy}}}\cos\left[\omega\left(t-\frac{r_{xy}\cos\theta}{c}\right)\right]d\theta\\ &= \frac{A^2}{2\pi}\int_0^{2\pi}\frac{e^{-2\alpha R}/R}{\sqrt{1-\frac{r_{xy}^2\cos^2\theta}{4R^2}}}\cos\left[\omega\left(t-\frac{r_{xy}\cos\theta}{c}\right)\right]d\theta\\ &\approx \frac{A^2}{2\pi}\int_0^{2\pi}\frac{e^{-2\alpha R}}{R}\cos\left[\omega\left(t-\frac{r_{xy}cos\theta}{c}\right)\right]d\theta\\ &= \frac{A^2e^{-2\alpha R}}{R}\cos(\omega t)\,J_0\left(\frac{\omega r_{xy}}{c}\right).\end{aligned} \tag{23}$$

Here, as elsewhere, C_{xy} is implicitly a function of t (unless otherwise stated) whereas $\hat{C}_{xy}$ is implicitly a function of ω.

[28] Perhaps surprisingly, despite the fact that attenuation has been accounted for, there is no dependence of C^E_{xy} on the station-station attenuation $e^{-\alpha r_{xy}}$. The reason for this is that the increase in attenuation due to the slightly longer source-station path is exactly compensated for by the decrease in attenuation due to the slightly shorter source-station path. Similarly, although the dependence on the Bessel function has been observed by many previous authors [e.g., *Aki*, 1957; *Sanchez-Sesma and Campillo*, 2006; *Tsai*, 2009], it may also be somewhat surprising that the geometrical attenuation inherent in the Bessel function (proportional to $1/\sqrt{r_{xy}}$ in the far-field) is captured despite the fact that far-field sources have a geometric attenuation ($e^{-2\alpha R}$) that is independent of the station-station spacing. Geometric attenuation is, nonetheless, captured because of the integral over noise sources.

[29] Similarly calculating C^E_{xx} yields

$$\begin{aligned}2C^E_{xx} &\approx \frac{A^2}{2\pi}\int_0^{2\pi}\frac{e^{-2\alpha r_{sx}}}{r_{sx}}\cos(\omega t)\,d\theta\\ &= \frac{A^2e^{-2\alpha R}}{2\pi R}\cos(\omega t)\int_0^{2\pi}\frac{e^{-\alpha r_{xy}\cos\theta}d\theta}{1-\cos\theta\cdot r_{xy}/(2R)}\\ &\approx \frac{A^2e^{-2\alpha R}}{R}\cos(\omega t)\,I_0(\alpha r_{xy}),\end{aligned} \tag{24}$$

where I_k is a modified Bessel function of the first kind, of order k. (The far-field assumption $R \gg r_{xy}$ has been used to simplify the integral.) The final expression for C^E_{yy} is identical to that for C^E_{xx}. Thus, the coherency as defined by equation (21) is given by

$$\hat{C}^E_{xy} = \frac{1}{I_0(\alpha r_{xy})}J_0\left(\frac{\omega r_{xy}}{c}\right). \tag{25}$$

[30] The fact that $I_0(x) \neq e^x$ implies that there is a significant difference between equation (25) and equation (22) (see Figure 2), and therefore that the *Prieto et al.* [2009] assumption of equation (22) may not be appropriate. (Note that in *Prieto et al.* [2009], $10^{-3} \lesssim \alpha r_{xy} \lesssim 2$, and that asymptotically $I_0(x) \to e^x/\sqrt{2\pi x}$.) In particular, if the true noise source distribution were close to the assumed uniform distribution of far-field surface waves then the attenuation parameters solved for using the *Prieto et al.* [2009] method must be reinterpreted before they can be directly compared with traditional (source-station) attenuation measurements. For this case, since equation (25) decays slower than equation (22), if one were to use equation (22) to infer α, one would obtain smaller values than the true α, and using these inferred values of α would result in ground motion predictions larger than true ground motions. However, the noise distribution chosen here may not be representative of true distributions and in the following sections we provide a few, perhaps more realistic, alternative examples.

3.1.2. One-Sided Far-Field Surface Waves

[31] In the case where noise sources are again uniformly distributed far-field surface-wave sources but are now only distributed along half of the circle (e.g. for $-\pi/2 < \theta < \pi/2$, see Figure 1b), then again equation (20) can be solved

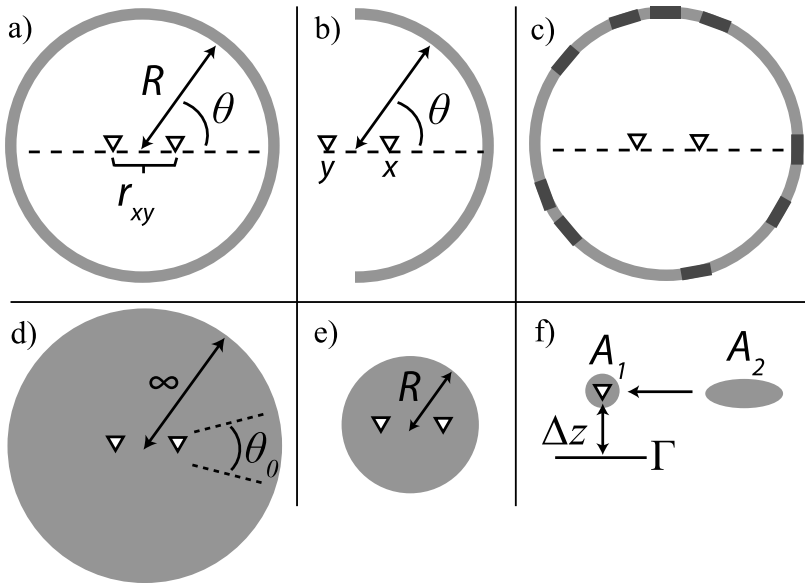

Figure 1. Schematic distributions of noise sources. The triangles denote the stations and the gray shaded area denotes the region of noise sources for the following cases: (a) uniform distribution of far-field surface waves, (b) one-sided far-field surface waves, (c) arbitrary non-uniform far-field surface waves, (d) uniform distribution of surface waves, (e) truncated uniform distribution of near-field surface waves, and (f) reflection geometry (see Appendix A). See text for description of variables.

in closed form for C^E_{xy}, C^E_{xx} and C^E_{yy}. This distribution may be approximately appropriate (in the microseism band, ≈5 – 30 s period) for stations that are relatively far away from any ocean, but where the coastline is much closer on one side compared to other, as for many station pairs in California [*Prieto et al.*, 2009]. Using the same approach as for equation (23), then

$$2C^E_{xy} \approx \frac{A^2 e^{-2\alpha R}}{\pi R} \Re\left[\int_{-\pi/2}^{\pi/2} e^{i\omega\left(t - r_{xy}\cos\theta/c\right)} d\theta\right]$$
$$= \frac{A^2 e^{-2\alpha R}}{R} \Re\left[e^{i\omega t} \cdot \left\{J_0\left(\frac{\omega r_{xy}}{c}\right) - iH_0\left(\frac{\omega r_{xy}}{c}\right)\right\}\right], \quad (26)$$

where H_0 is a Struve function of order zero [*Watson*, 1952]. (Note that Struve functions are often denoted with a bold $\boldsymbol{H}_k$ and are not equivalent to Hankel functions, $H^{(i)}_k$.) Similarly,

$$2C^E_{xx} \approx \frac{A^2 e^{-2\alpha R}}{\pi R} \cos(\omega t) \int_{-\pi/2}^{\pi/2} e^{-\alpha r_{xy}\cos\theta} d\theta$$
$$= \frac{A^2 e^{-2\alpha R}}{R} \cos(\omega t) \left[I_0\left(\alpha r_{xy}\right) - L_0\left(\alpha r_{xy}\right)\right], \quad (27)$$

$$2C^E_{yy} \approx \frac{A^2 e^{-2\alpha R}}{\pi R} \cos(\omega t) \int_{-\pi/2}^{\pi/2} e^{\alpha r_{xy}\cos\theta} d\theta$$
$$= \frac{A^2 e^{-2\alpha R}}{R} \cos(\omega t) \left[I_0\left(\alpha r_{xy}\right) + L_0\left(\alpha r_{xy}\right)\right], \quad (28)$$

where L_0 is a modified Struve function of order zero [*Watson*, 1952]. The coherency is then given by

$$\hat{C}^E_{xy} = \frac{J_0\left(\frac{\omega r_{xy}}{c}\right) + iH_0\left(\frac{\omega r_{xy}}{c}\right)}{\sqrt{I_0^2\left(\alpha r_{xy}\right) - L_0^2\left(\alpha r_{xy}\right)}}. \quad (29)$$

Equation (29) also decays more slowly with increasing r_{xy} compared to equation (22) (see Figure 2). If one were to use equation (22) to infer α in a case where this one-sided far-field distribution were appropriate, again one would infer values lower than the true values of α and predict ground motions larger than the true ground motions.

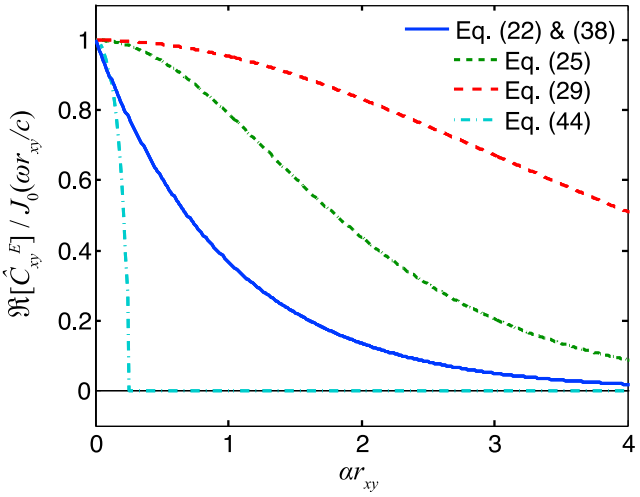

Figure 2. Comparisons of $\Re[\hat{C}^E_{xy}]/J_0(\omega r_{xy}/c)$ for equation (22) (blue solid), equation (25) (green dotted), equation (29) (red dashed), and equation (44) (cyan dash-dotted).The blue curve is the assumption of the *Prieto et al.* [2009] as well as the result of equation (38) for uniform noise everywhere (see Figure 1d); the green curve is for uniform far-field noise (see Figure 1a); the red curve is for uniform one-sided far-field noise (see Figure 1b); the cyan curve is for uniform near-field noise (with $\alpha R = 1/8$) (see Figure 1e). As described in the text, $\alpha = \omega/(2UQ)$.

3.1.3. Arbitrary Distribution of Far-Field Surface Waves

[32] Given an arbitrary distribution of far-field surface waves (see Figure 1c), we can also solve equation (20) in closed form, in terms of a sum over Bessel functions as in the work of *Cox* [1973] or *Harmon et al.* [2010]. Writing the square of the azimuthal source distribution $A_s^2(\theta)$ as a Fourier series

$$A_s^2(\theta) = \sum_{k=0}^{\infty} a_k \cos(k\theta) + b_k \sin(k\theta), \tag{30}$$

and substituting into equation (20) yields

$$\begin{aligned} 2C_{xy}^E &\approx \frac{1}{2\pi R}\Re\left[\int_0^{2\pi} A_s^2 e^{-\alpha\left(r_{sx}+r_{sy}\right)} e^{i\omega\left(t-r_{xy}\cos\theta/c\right)} d\theta\right] \\ &= \frac{e^{-2\alpha R}}{2\pi R}\Re\left[e^{i\omega t}\int_0^{2\pi} A_s^2(\theta)\, e^{-i\omega r_{xy}\cos\theta/c} d\theta\right] \\ &= \frac{e^{-2\alpha R}}{R}\Re\left[e^{i\omega t}\sum_k (-i)^k a_k J_k\left(\frac{\omega r_{xy}}{c}\right)\right]. \end{aligned} \tag{31}$$

Similarly,

$$\begin{aligned} 2C_{xx}^E &\approx \frac{1}{2\pi R}\int_0^{2\pi} A_s^2(\theta)\, e^{-2\alpha r_{xx}} \cos[\omega t]\, d\theta \\ &= \frac{e^{-2\alpha R}}{2\pi R}\cos(\omega t)\int_0^{2\pi} A_s^2(\theta)\, e^{-\alpha r_{xy}\cos\theta} d\theta \\ &= \frac{e^{-2\alpha R}}{R}\cos(\omega t)\sum_k (-1)^k a_k I_k\left(\alpha r_{xy}\right) \end{aligned} \tag{32}$$

$$\begin{aligned} 2C_{yy}^E &\approx \frac{e^{-2\alpha R}}{2\pi R}\cos(\omega t)\int_0^{2\pi} A_s^2(\theta)\, e^{\alpha r_{xy}\cos\theta} d\theta \\ &= \frac{e^{-2\alpha R}}{R}\cos(\omega t)\sum_k a_k I_k\left(\alpha r_{xy}\right). \end{aligned} \tag{33}$$

The coherency is then

$$\hat{C}_{xy}^E = \frac{\sum_k i^k a_k J_k\left(\frac{\omega r_{xy}}{c}\right)}{\sqrt{\sum_k a_k I_k\left(\alpha r_{xy}\right)}\sqrt{\sum_k (-1)^k a_k I_k\left(\alpha r_{xy}\right)}}, \tag{34}$$

and the real part of the coherency is

$$\Re\left[\hat{C}_{xy}^E\right] = \frac{\sum_k (-1)^k a_{2k} J_{2k}\left(\frac{\omega r_{xy}}{c}\right)}{\sqrt{\sum_k a_k I_k\left(\alpha r_{xy}\right)}\sqrt{\sum_k (-1)^k a_k I_k\left(\alpha r_{xy}\right)}}. \tag{35}$$

[33] It is clear from comparison that equation (35) and equation (22) can be even more dissimilar than the previous comparisons. In particular, for non-uniform distributions of noise, the dependence of the real part of the coherency on $J_0(\omega r_{xy}/c)$ is destroyed so that the differences are not relegated completely to a function of αr_{xy} as they were in sections 3.1.1 and 3.1.2. As previously noted [e.g., *Tsai*, 2009; *Harmon et al.*, 2010], this non-J_0 dependence results in biased phase velocities if not accounted for. Focusing instead on the amplitudes, we note that the general shape of the curves are similar since all J_{2k} are asymptotically equal to $\pm J_0$. Unfortunately, this also means that a non-uniform distribution of noise can superficially look somewhat like the expected effects of attenuation, even when attenuation does not exist. As a simple example of this, we consider the case where $\alpha = 0$, $a_0 = 1$, $a_2 = -0.3$, and all other a_k are zero. In this case, equation (35) gives $\Re[\hat{C}_{xy}^E] = J_0(\omega r_{xy}/c) + 0.3J_2(\omega r_{xy}/c)$ (see Figure 3). This curve resembles $J_0(\omega r_{xy}/c)$ except that the amplitude decreases with increasing r_{xy} so that one could mistakenly fit this with an attenuation model. Interestingly, if the sign on a_2 were positive, one would infer a negative attenuation. Fortunately, though, both of these errors can be easily avoided by using azimuthal averages. If an azimuthal average is done (with all azimuths contributing equally), then the resulting $\hat{C}_{xy}^E$ will have an equal contribution from terms with positive and negative coefficients a_k (for $k > 0$) and therefore will be left only with the a_0 term and the corresponding J_0 term.

[34] With $\alpha \neq 0$, there will still remain a difference in the decay of the azimuthally averaged coherency for different distributions of noise due to the denominator of equation (35). However, for reasonable values of $\omega r_{xy}/c$ and α, this difference is relatively small, and the decay of coherency can be approximated with one of the curves in Figure 2. For example, for the case just discussed with $a_0 = 1$, $a_2 = -0.3$, an azimuthal average of coherency including $\alpha \neq 0$ will result in a decay that is almost equal to $1/I_0(\alpha r_{xy})$ and is bounded by $1/[I_0(\alpha r_{xy}) + 0.3I_2(\alpha r_{xy})]$ and $1/[I_0(\alpha r_{xy}) - 0.3I_2(\alpha r_{xy})]$, two functions that are not too different. Similarly, performing an azimuthal average on the one-sided distribution of section 3.1.2 would result in an azimuthally averaged $\Re[\hat{C}_{xy}^E]$ that is bounded by equation (25) and equation (29).

3.1.4. Including Near-Field Surface Waves

[35] The opposite end-member case to far-field surface-wave noise sources are surface-wave noise sources that encompass the near-field region surrounding the stations. Unlike the far-field case where sources can effectively be assumed to be distributed in an azimuthal distribution (A_s is only a function of azimuth θ), for this case, the full 2D distribution of sources must be accounted for so that $A_s \equiv A(\boldsymbol{s}) = A(r, \theta)$ (see Figure 1d). This distribution of noise may be appropriate for island stations that are well surrounded by nearby oceanic microseism [*McNamara and Buland*, 2004].

[36] For $A_s = A$ is constant everywhere, *Snieder* [2007] has shown that the cross correlation is equal to the extended Green's function (the sum of positive and negative Green's functions) divided by the local attenuation rate. In the language used here for the 2D case, this equality can be expressed as

$$2C_{xy}^E = \frac{2A^2}{\alpha} e^{-\alpha r_{xy}} \cos(\omega t)\, J_0\left(\frac{\omega r_{xy}}{c}\right), \tag{36}$$

where (as before) α is still assumed to be small. Taking $x = y$ yields

$$2C_{xx}^E = 2C_{yy}^E = \frac{2A^2}{\alpha}\cos(\omega t). \tag{37}$$

The coherency is therefore given by

$$\hat{C}_{xy}^E = e^{-\alpha r_{xy}} J_0\left(\frac{\omega r_{xy}}{c}\right). \tag{38}$$

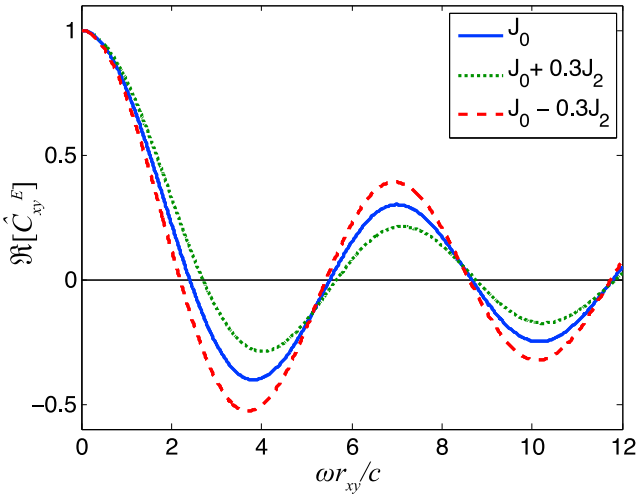

Figure 3. Comparison of $\Re[\hat{C}^E_{xy}]$, for a uniform distribution of far-field noise sources (solid blue curve) and 2 examples of a non-uniform distribution of far-field noise sources (dotted green and dashed red curves). The 2 non-uniform distributions are for $A_s^2(\theta) = 1 \mp 0.3\cos(2\theta)$, respectively. One may note that the green curve decays faster with r_{xy} than the uniform case (blue curve) and could be misinterpreted as being due to attenuation.

In this special case of uniformly distributed noise sources, equation (38) is identically equal to equation (22) and we therefore find that the *Prieto et al.* [2009] assumption of equation (22) is appropriate (see Figure 2). (A less general result for 3D isotropic waves was also previously shown by *Roux et al.* [2005].)

[37] When A_s varies azimuthally (but covers the entire 2D plane), the result of *Snieder* [2007] can no longer be applied directly, and we resort to calculations like the ones of previous sections. This analysis not only gives insight into how expressions like equation (36) arise but also provide approximate results when A_s varies azimuthally. As shown in Appendix B, an approximation for C^E_{xy} can be made by observing that only a relatively narrow beam of azimuths θ_0 contributes strongly to C^E_{xy} [*Snieder*, 2004]. With a constant amplitude $A_s \equiv A_\theta$ within this beam (see Figure 1d), then

$$2C^E_{xy} \approx \frac{2A_\theta^2}{\alpha} e^{-\alpha r_{xy}} \cos(\omega t)\, J_0\left(\frac{\omega r_{xy}}{c}\right). \tag{39}$$

[38] On the other hand, the autocorrelation C^E_{xx} does not have this beamed sensitivity, but is instead equally sensitive to noise sources in all directions. Assuming that the average value of A_s^2 is given by $\overline{A}^2$, then C^E_{xx} is approximately given by

$$2C^E_{xx} \approx \frac{2\overline{A}^2 \cos(\omega t)}{\alpha}, \tag{40}$$

and the same for C^E_{yy} (assuming approximately the same azimuthal variation can be applied for both x and y). The coherency can then easily be calculated as

$$\hat{C}^E_{xy} = \frac{A_\theta^2}{\overline{A}^2} e^{-\alpha r_{xy}} J_0\left(\frac{\omega r_{xy}}{c}\right). \tag{41}$$

[39] One final point worth mentioning is that the preceding discussion explains why both the cross correlation and the coherency have a dependence on $e^{-\alpha r_{xy}}$. The qualitative reason for this is that while the cross correlation amplitude decays with distance as $e^{-\alpha r_{xy}}$, the autocorrelation is constant due to the sum over all sources. Thus, unlike all of the far-field cases discussed before, in this case the coherency is simply a scaled version of the cross correlation, and its form is not affected by the division described by equation (21).

3.1.5. Truncated Distribution of Near-Field Surface Waves

[40] In this section, we consider the same uniform distribution of near-field surface waves discussed in the previous section except here we assume that this distribution is truncated at a radius R that is small compared to the attenuation distance $1/\alpha$ (see Figure 1e). Since ocean microseism may be more strongly excited close to the coast and not as strongly excited in deep water [*Bromirski and Duennebier*, 2002], this distribution of noise may be more appropriate than that of section 3.1.4 for island stations that are well surrounded by oceanic microseism.

[41] Since $R \ll 1/\alpha$, attenuation is negligible and can be ignored. As in Appendix B, we use the far-field approximation despite having near-field sources. After providing this approximate solution, we compare with a numerical calculation with the exact solution. Integrating only the sources within the (now truncated) triangular beam, as in Appendix B, results in

$$\begin{aligned} 2C^E_{xy} &\approx A_\theta^2 \cos(\omega t)\, J_0\left(\frac{\omega r_{xy}}{c}\right) \int_{r_{xy}/2}^{R} \frac{2\pi r\, dr}{\sqrt{r^2 - r_{xy}^2/4}} \\ &= 2\pi A_\theta^2 \cos(\omega t)\, J_0\left(\frac{\omega r_{xy}}{c}\right) \sqrt{R^2 - r_{xy}^2/4}, \end{aligned} \tag{42}$$

and similarly,

$$\begin{aligned} 2C^E_{xx} &= \overline{A}^2 \cos(\omega t) \int_0^R \int_0^{2\pi} \frac{r\, d\theta\, dr}{\sqrt{r^2 + \frac{r_{xy}^2}{4} - r r_{xy}\cos(\theta)}} \\ &\approx \overline{A}^2 \cos(\omega t) \int_0^R \int_0^{2\pi} d\theta\, dr \approx 2\pi R \overline{A}^2 \cos(\omega t), \end{aligned} \tag{43}$$

where the approximation $r_{xy} \ll R$ is taken to evaluate equation (43). This approximation may be valid since the expressions are only used for $r_{xy} < 2R$ (under the same approximation, $C^E_{xy} = 0$ for $R < r_{xy}/2$). The coherency is then given by

$$\hat{C}^E_{xy} \approx \frac{A_\theta^2}{\overline{A}^2} \sqrt{1 - \frac{r_{xy}^2}{4R^2}} \cdot J_0\left(\frac{\omega r_{xy}}{c}\right), \tag{44}$$

again, only for $R > r_{xy}/2$ (and with $\hat{C}^E_{xy} = 0$ for $R < r_{xy}/2$). Intuitively, one can understand the decay of coherency with station spacing being due to the fact that there are fewer and fewer noise sources within the 2 beams of angular size θ_0 as r_{xy} increases (but R remains fixed), whereas there are the same number of total noise sources (contributing to C^E_{xx}).

[42] The form of equation (44) is significantly different than any of the previous expressions for coherency. In particular, for this distribution of noise, the coherency drops

dramatically (faster than exponentially) with increasing r_{xy} due to the lack of sources in the stationary-phase beams. See Figure 2 for comparison (for this figure, a relatively large value of $\alpha R = 1/8$ is chosen). Since the decay is faster than exponential, using equation (22) to infer α in this case would result in values larger than the true values of α. Using these inferred values of α, one would therefore predict ground motions smaller than true ground motions.

[43] As noted previously, we have used the far-field approximation in this calculation, despite near-field sources existing. To test the validity of this approximation, we compare the cross correlation estimated by equation (42) with numerical calculations using the both the exact equation (2) and the approximate equation (3). Using equation (2), the cross correlation in this case (with $\alpha = 0$) can be expressed as

$$C^E_{xy} \propto \Re\left[\int_0^R \int_0^{2\pi} rH_0^{(1)}\left(\frac{\omega r_+}{c}\right) H_0^{(2)}\left(\frac{\omega r_-}{c}\right) e^{-i\omega t} d\theta dr\right], \quad (45)$$

where $H_0^{(2)}$ is a Hankel function of the second kind and $r_\pm = \sqrt{r^2 + r_{xy}^2/4 \pm r r_{xy}\cos\theta}$, whereas using equation (3), the cross correlation can be expressed as

$$C^E_{xy} \propto \Re\left[\int_0^R \int_0^{2\pi} \frac{cr}{\omega\sqrt{r_+ r_-}} e^{i\omega\left[(r_+ - r_-)/c - t\right]} d\theta dr\right]. \quad (46)$$

The relative amplitudes of equation (42), equation (45) and equation (46) are plotted numerically in Figure 4 for three different choices of ω/c. Numerical integration is performed using an adaptive Gauss-Kronrod rule along with Duffy's coordinate transform [*Duffy*, 1982] and the IMT transformation [*Iri et al.*, 1987] as necessary. As can be seen, equation (46) agrees extremely well with equation (45), with errors always being less than 5%. Equation (42) is seen to be somewhat poorer of an approximation, and the primary error in equation (42) is therefore not due to using the far-field approximation but is instead due to the approximate integration. Equation (42) nevertheless provides a reasonable first-order understanding of how amplitudes decay in this near-field case (particularly when $r_{xy}/R < 1$).

3.1.6. Understanding *Cupillard and Capdeville* [2010] Results

[44] *Cupillard and Capdeville* [2010] present numerical noise correlation experiments with 3 different distributions of noise: one case with uniform 2D noise, one with a big (but finite) patch of noise sources, and one with a small patch of sources. These numerical experiments go beyond other previous work by properly accounting for a realistic Earth geometry and attenuation, and the amplitude results can therefore be directly compared with the general theoretical framework presented here.

[45] We first observe that since whitening is equivalent to division by the spectrum prior to cross correlation, the results for whitening should be identical to our coherency results, as calculated using equation (21). Thus, the calculations done in the previous sections can be used to compare both the 'raw' and 'whitened' results of *Cupillard and Capdeville* [2010]. Unfortunately, the '1-bit' results are more difficult to describe using the present framework and will not be discussed.

[46] The uniform 2D case is easily understood as being analogous to the uniform 2D case discussed in section 3.1.4. In this case, *Cupillard and Capdeville* [2010] observe that both the 'raw' correlations and the 'whitened' correlations have amplitudes that decay as expected of the Green's function. Within the present framework, in section 3.1.4, we have shown that both the cross correlation and the coherency have amplitudes that decay as expected for the Green's function, thus explaining the observations of *Cupillard and Capdeville* [2010].

[47] The 'small patch' example is also easily understood as being analogous to the 1-source case discussed in section 2.1 and shown in Table 1. The decay of amplitude with $\epsilon(r_{1x})\epsilon(r_{1y})$ is exactly that shown by *Cupillard and Capdeville* [2010] to fit the observed decay of the 'raw' correlation. For the 'whitened' correlation, our coherency results suggest no decay with station-station spacing (see Table 1). The reason *Cupillard and Capdeville* [2010] still observe a decay with distance is that they normalize their results relative to (what we call) $C^E_{xx}(\omega)$ rather than $\sqrt{C^E_{xx}C^E_{yy}}$. One may observe that for a uniform distribution of noise sources, $C^E_{xx} = C^E_{yy}$ as shown in equation (37), but that this equality no longer holds for non-uniform sources. One may also note that our results also contain the $\pi/4$ phase shift (between the cos dependence of $\Re[\hat{C}^E_{xy}]$ and the asymptotic form of J_0).

[48] The 'big patch' example is not as easily understood, but perhaps can be very roughly approximated using a 'uniform but one-sided 2D' distribution of sources. While this case is not explicitly considered above, the analysis in section 3.1.4 and Appendix B suggests that in this case the real part of $C^E_{xy}(\omega)$ would have the same form as equation (36). The fact that the 'raw' correlation has the correct total attenuation is therefore understood. On the other hand, the coherency is affected because (while C^E_{xx} remains constant) C^E_{yy} decreases as the second station is moved farther from the noise sources. In fact, just as for the 'small patch' example, C^E_{yy} decays approximately as $\epsilon(\bar{r}_{sy})^2$, where $\bar{r}_{sy}$ is an average source-station distance. It is unclear if the precise form of this decay accounts exactly for the observed mismatch for the 'whitened' example described by *Cupillard and Capdeville* [2010], but it at least has a qualitatively similar form.

3.1.7. Summary of Section 3.1

[49] In sections 3.1.1–3.1.5, we have shown how the coherency depends on various assumed noise source distributions. A summary of the cross correlation, autocorrelation and coherency results for the different cases considered is summarized in Table 1. We find that for all of the source distributions considered, the amplitude dependence (beyond the $J_0(\omega r_{xy}/c)$ term) can generally be written as a function of αr_{xy} and that this function generally decreases with increasing αr_{xy}, as plotted in Figure 2. However, the functional forms of this decay are substantially different depending on the exact distribution of noise sources. For this reason, without first determining which source distribution best approximates a given situation in reality, it is not possible to quantitatively relate coherency measurements to attenuation parameters. We suggest that researchers interested in performing attenuation measurements from noise correlation measurements should first determine how the dominant sources of noise are distributed. Determining this source distribution may not be easy, and is complicated by the fact that the source distributions we discuss include any secondary

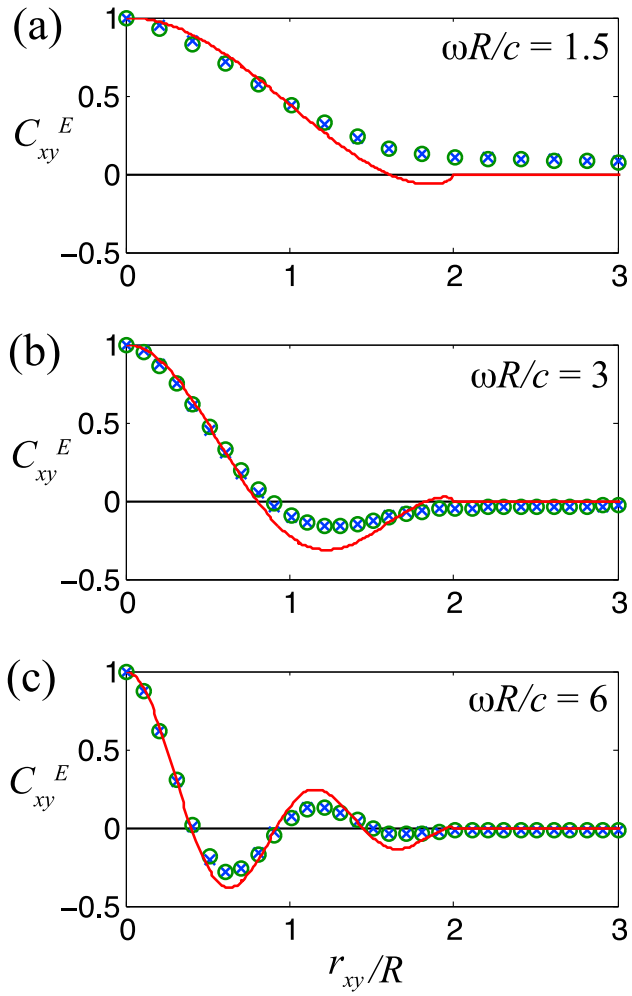

Figure 4. Comparison of (normalized) C^E_{xy} for equation (42), equation (45) and equation (46), for 3 different choices of ω/c. In all 3 panels, the exact result of equation (45) is plotted as blue crosses, numerical integration of the far-field approximation equation (46) is plotted as green circles, and the approximate integration of equation (42) is plotted as a red line. (a) $\omega R/c = 1.5$, (b) $\omega R/c = 3$, (c) $\omega R/c = 6$. In all cases, there is excellent agreement between equation (45) and equation (46) and there is rough agreement between those and equation (42). Note that all sources are interior to the stations when $r_{xy}/R > 2$.

sources such as scatterers. If scattering is significant and scatterers are well distributed (as might be expected of many regions), scattering would contribute to a more homogeneous source distribution than would be expected of a given primary source distribution.

[50] In section 3.1.6, we showed that some of the numerical results of *Cupillard and Capdeville* [2010] can be understood using the framework provided. This successful agreement between the theoretical framework and the numerical experiments strongly suggests that the results presented here are useful as a good approximation to reality.

3.2. Signal-to-Noise Ratios

[51] Given the results of section 2, it is straightforward to compute a signal-to-noise ratio, *SNR*. The 'noise' is simply the sum of incoherent arrivals, and is given by the sum of all terms in C^E_{xyM} that are multiplied by $1/\sqrt{M}$; on the other hand, the 'signal' is simply the sum of coherent arrivals, and is given by all remaining terms not multiplied by $1/\sqrt{M}$. The *SNR* is then just the ratio of the amplitude of the 'signal' to the amplitude of the 'noise,' and the requirement on retrieving a robust signal is that SNR $\gtrsim 1$. Since $\sqrt{M} \propto \sqrt{T_0}$, the *SNR* generally increases as $\sqrt{T_0}$, a fact that has been pointed out previously by a number of authors [e.g., *Snieder*, 2004; *Sabra et al.*, 2005b]. However, this other work has not quantified the specific dependence of the *SNR* on certain key parameters or in situations where the noise distribution is non-uniform. In the following sections, we provide full expressions for the *SNR* for a few different noise distributions as well as the requirements in these cases for obtaining a robust signal. While it may be difficult to estimate which simplified case best corresponds to a given deployment, the results presented here at least provide guidance to the range of possible results.

3.2.1. Two Sources

[52] First, we consider the simplest (primarily pedagogical) case where there are just two noise sources. In this case, C^E_{xyM} is given by equation (14). As noted in section 2.2, this very limited case already roughly approximates the case for high-frequency surface waves since high-frequency surface waves are primarily sensitive to noise sources at the 2 stationary phase points [*Snieder*, 2004]. In this case, it is also assumed that there exists no other sources of observed displacements beyond these two sources (including incoherent sources). This assumption is appropriate if the vast majority of cross correlation noise is in the form of elastic energy.

[53] Assuming that the 2 coherent terms have very different arrival times, then the *SNR* should be calculated separately for the 2 terms. Inherent in this statement is an assumption that one actually has a narrow band of frequencies rather than a single frequency such that different groups of arrivals can be examined separately. Taking this assumption, then the ratio of amplitudes yields

$$SNR_1 = \frac{A_1^2 \epsilon(r_{1x})\,\epsilon(r_{1y})}{A_1 A_2/\sqrt{M}\cdot\sqrt{\epsilon^2(r_{1y})\,\epsilon^2(r_{2x}) + \epsilon^2(r_{2y})\,\epsilon^2(r_{1x})}} = \frac{A_1 \epsilon(r_{1x})\,\epsilon(r_{1y})}{A_2\sqrt{\epsilon^2(r_{1y})\,\epsilon^2(r_{2x}) + \epsilon^2(r_{2y})\,\epsilon^2(r_{1x})}}\sqrt{\frac{T_0}{T_a}}, \tag{47}$$

where SNR_1 is the signal-to-noise ratio for the first coherent arrival, and SNR_2 is the same expression with 1's and 2's switched. Note that the noise amplitudes are added in a root mean square sense. When all of the $\epsilon(r)$ terms are equal, the expression simplifies to

$$SNR_1 = \frac{A_1}{\sqrt{2}A_2}\sqrt{\frac{T_0}{T_a}}. \tag{48}$$

[54] In this case of equation (48), the requirement for T_0 to retrieve a robust signal is that

$$T_0 \gtrsim 2T_a \cdot \frac{A_2^2}{A_1^2}. \tag{49}$$

There are a few points to note about this result. First, the total length of correlation time needed is proportional to the

attenuation time T_a. This is a general feature of all results in this section due to the fact that $M = T_0/T_a$ is the only place that T_0 and T_a appear and that the *SNR* in all expressions is proportional to $\sqrt{M}$. Second, as $A_2/A_1 \rightarrow 0$, T_0 can be shorter and shorter (approaching zero). This can be rationalized because in that limit, there is only one source and hence there are no cross terms and hence there is no 'noise.' Finally, one may note that if $A_1 = A_2$ then T_0 must be at least twice as long as T_a to retrieve a robust signal (for both coherent terms).The 2 is related to the 2 incoherent terms (for N terms, the appropriate coefficient would be $N^2 - N$ as discussed in section 2.4).

3.2.2. Far-Field Surface Waves

[55] In calculating signal-to-noise ratios, it is important to use the same units to treat both the coherent and incoherent terms. Thus, in using equation (23), we must recognize that the A^2 in that expression is equivalent to NA_j^2 if a limit of equation (19) were used instead. Substituting equation (23) into equation (19) with this modification then results in

$$2C^E_{xyM} = NA_j^2 \frac{e^{-2\alpha R}}{R}\cos(\omega t)\, J_0\left(\frac{\omega r_{xy}}{c}\right) + \frac{N}{\sqrt{M}}\overline{A}^2 \frac{e^{-2\alpha R}}{R}\cos[\omega t + \phi^{av}]. \quad (50)$$

Here we note that if the noise distribution is uniform, then $A_j = \overline{A}$. On the other hand, a non-uniform distribution of far-field surface-wave noise can be approximately accounted for by simply letting $A_j \neq \overline{A}$. The coherent term amplitude, A_j, can be interpreted as the average amplitude of noise sources within the beam pointing in the station-station direction, $\theta = 0$ and of angular size θ_0 (see equation (B2) of Appendix B). We therefore replace A_j by A_θ, where A_θ depends on the azimuth of the station-station direction. On the other hand, the incoherent term amplitude, $\overline{A}^2$, can be interpreted as the average product of amplitudes of noise sources in all directions, as in section 2.4. Since the amplitude of $J_0(x)$ asymptotically decays as $\sqrt{2/\pi x}$, then

$$SNR \approx \frac{A_\theta^2}{\overline{A}^2}\sqrt{\frac{2c}{\pi\omega r_{xy}}\cdot\frac{T_0}{T_a}}, \quad (51)$$

where this expression is appropriate for $\omega r_{xy}/c \gg 1$, and the requirement $SNR \gtrsim 1$ gives

$$T_0 \gtrsim \frac{\pi\omega r_{xy}}{2c}\cdot\frac{\overline{A}^4}{A_\theta^4}\cdot T_a. \quad (52)$$

[56] This expression has a few key dependencies. First, it shows that as $\omega r_{xy}/c$ increases, that T_0 must increase linearly, as long as T_a remain constant. (Note that as discussed below, T_a may be inversely proportional to ω.) The reason for this dependency is that the beam of angular size θ_0 discussed in the Appendix gets narrower as $\omega r_{xy}/c$ increases and therefore the region of coherence gets smaller.

[57] Secondly, the dependence on $\overline{A}/A_\theta$ to the fourth power means that relatively small differences in the relative average amplitudes can have a significant impact on the requirement on T_0.

[58] Finally, equation (52) depends linearly on T_a. In order to estimate how long T_0 must be, we must have an estimate of T_a. As a reminder, T_a is the attenuation time of the physical system that generates the noise sources and is therefore different for different physical processes. For example, T_a for ocean microseism would be related to the length of time it takes for the phase of ocean waves to shift by a significant fraction of a period. In the absence of any real data on T_a for ocean waves, it may be reasonable to assume that this time is longer than a single period but not longer than a large number of periods. Making this assumption of $T_a \approx 10T_\omega = 20\pi/\omega$, where T_ω is the period of the wave, then now one has all the parameters needed to estimate T_0 from equation (52). Before performing this estimate, we observe that if $T_a \approx 10T_\omega = 20\pi/\omega$ is a good approximation, then the dependence on ω drops out of the *SNR* as well as the requirement on T_0. Taking the example of a uniform distribution of 10-second ocean microseism observed at stations separated by $r_{xy} = 50$ km then $c \approx 3$ km/s, $\overline{A}/A_\theta = 1$, $T_a \approx 100$ s, $\omega r_{xy}/c \approx 10$, yielding $T_0 \gtrsim 27$ min as a requirement on the signal to be larger than the noise. It is known that noise correlation measurements can be successful on as little as a few days of data [*Brenguier et al.*, 2008]. If the calculation just done is approximately correct, then $T_0 \approx 2$ days would correspond to $SNR \approx 9$, which indeed may be a reasonable *SNR* for a (very) robust signal.

3.2.3. Including Near-Field Surface Waves

[59] For this case, all noise amplitudes (A_s or A) are such that A_s^2 or A^2 have units of amplitude squared times distance per unit area. With the same interpretation for A_θ as before, equation (39) with equation (20) gives C^E_{xyM} as

$$2C^E_{xyM} \approx \frac{2A_\theta^2 e^{-\alpha r_{xy}}}{\alpha}\cos(\omega t)\, J_0\left(\frac{\omega r_{xy}}{c}\right) + \frac{N\overline{A}^2 l_c^2}{\sqrt{M} r_{av}}\cos[\omega t + \phi^{av}], \quad (53)$$

where l_c is a correlation length that defines the size of each of the N regions within which sources are dependent, N is an effective number that accounts for attenuation, and r_{av} is an average source-station distance. Accounting for the Bessel function decay as before, then

$$SNR \approx \frac{2e^{-\alpha r_{xy}} r_{av}}{N l_c^2 \alpha}\frac{A_\theta^2}{\overline{A}^2}\sqrt{\frac{2c}{\pi\omega r_{xy}}\cdot\frac{T_0}{T_a}}, \quad (54)$$

where, as before, we have taken $\omega r_{xy}/c \gg 1$. Given a total source region of area L^2, then one may estimate $N \approx L^2/l_c^2$. The effective source area L^2 can be determined by integrating the amplitude term as in section 3.1.4 so that

$$\frac{L^2}{r_{av}} = \int_s \frac{2e^{-2\alpha r_{sx}}}{\pi r_{sx}} ds = \int_{r=0}^{\infty}\int_{\theta=0}^{2\pi} \frac{2re^{-2\alpha r_{sx}}}{\pi r_{sx}} d\theta dr = \int_{r=0}^{\infty} 4e^{-2\alpha r} dr = \frac{2}{\alpha}. \quad (55)$$

Using this expression for L^2/r_{av}, equation (54) simplifies to

$$SNR \approx e^{-\alpha r_{xy}}\frac{A_\theta^2}{\overline{A}^2}\sqrt{\frac{2c}{\pi\omega r_{xy}}\cdot\frac{T_0}{T_a}}. \quad (56)$$

[60] Solving for the robust signal requirement ($SNR \gtrsim 1$) yields

$$T_0 \gtrsim e^{2\alpha r_{xy}} \frac{\pi \omega r_{xy}}{2c} \cdot \frac{\overline{A}^4}{A_\theta^4} \cdot T_a. \tag{57}$$

In addition to the dependencies discussed in section 3.2.2, this expression has an added dependence on αr_{xy} such that T_0 increases as the inverse square of the attenuation term $e^{-\alpha r_{xy}}$. The reason for this dependence is that the coherent signal (from near-field waves) decays exponentially with station separation but the incoherent signal (from these same waves) does not decay. Therefore, as the station spacing increases, one must have a longer correlation time in order to obtain a robust signal. For the same example discussed previously of 10-second waves observed at r_{xy} = 50 km, $\alpha \approx 2 \cdot 10^{-6}$ m^{-1} [e.g., *Prieto et al.*, 2009] so that $e^{2\alpha r_{xy}} \approx 1.2$, and T_0 is nearly unaffected by this term. However, if r_{xy} = 500 km, then $e^{2\alpha r_{xy}} \approx 7.4$ and T_0 would need to be a factor of 7.4 times longer to achieve the same *SNR*.

3.2.4. Truncated Distribution of Near-Field Surface Waves

[61] For a truncated distribution of near-field surface waves as discussed in section 3.1.5, adding the incoherent terms to equation (42) while still allowing for A_θ and $\overline{A}$ to be different results in

$$2C^E_{xyM} \approx 2\pi A_\theta^2 \cos(\omega t)\, J_0\left(\frac{\omega r_{xy}}{c}\right) \sqrt{R^2 - r_{xy}^2/4} + \frac{N\overline{A}^2 l_c^2}{\sqrt{M} r_{av}} \cos[\omega t + \phi^{av}], \tag{58}$$

where, as before, l_c^2 approximately accounts for the size of each of the N regions and r_{av} is an average source-station distance. Accounting for the Bessel function decay as before, then

$$SNR \approx \frac{2\pi r_{av}\sqrt{R^2 - r_{xy}^2/4}\, A_\theta^2}{N l_c^2 \overline{A}^2} \sqrt{\frac{2c}{\pi \omega r_{xy}} \cdot \frac{T_0}{T_a}}. \tag{59}$$

Setting $N \approx \pi R^2 / l_c^2$ and $1/r_{av} = 2/R$ then equation (59) simplifies to

$$SNR \approx \sqrt{1 - \left(\frac{r_{xy}}{2R}\right)^2} \frac{A_\theta^2}{\overline{A}^2} \sqrt{\frac{2c}{\pi \omega r_{xy}} \cdot \frac{T_0}{T_a}}. \tag{60}$$

Noting again that we have assumed $R > r_{xy}/2$, then one can solve for the requirement on R to retrieve a robust signal

$$R \gtrsim \frac{r_{xy}}{2\sqrt{1 - \left(\frac{\pi \omega r_{xy}}{2c} \cdot \frac{\overline{A}^4}{A_\theta^4} \cdot \frac{T_a}{T_0}\right)}}. \tag{61}$$

Note that if T_0 is too short then the term in parentheses in equation (61) will be larger than 1, leaving the domain of possibility (i.e. $R > \infty$). Also, it should be noted that if R is required to be too large, then the assumption that $R \ll 1/\alpha$ will not be satisfied and one should use a different model for the distribution of noise sources.

3.2.5. Including Incoherent Terms

[62] So far, the entire incoherent signal has been assumed to be a sum over products of coherent terms only so that equation (18) can be approximated by equation (19) (i.e. all 'noise' is realization noise). However, it is unclear whether the criteria $A_{Ix} \ll NA_{av}\,\epsilon(r_x^{av})$ and $A_{Iy} \ll NA_{av}\epsilon(r_y^{av})$ required for this approximation to hold are always satisfied. For example, some seismic stations are prone to especially large local effects, especially in certain frequency bands [e.g., *Tsai et al.*, 2004; *Berger et al.*, 2004; *Zurn et al.*, 2007]. Fortunately, it is straightforward to include these terms simply by using the un-approximated equation (18) instead of equation (19). Doing so, for example, would modify equation (56) to become

$$SNR \approx \frac{e^{-\alpha r_{xy}} A_\theta^2 \sqrt{\frac{2c}{\pi \omega r_{xy}} \cdot \frac{T_0}{T_a}}}{\sqrt{\overline{A}^4 + \frac{2}{\alpha}\overline{A}^2 \left(A_{Ix} + A_{Iy}\right)^2 + \frac{4}{\alpha^2} A_{Ix}^2 A_{Iy}^2}}, \tag{62}$$

where it should be noted that the units of A_θ and $\overline{A}$ (for this 2D case) are such that A_θ^2 and $\overline{A}^2$ have units of amplitude squared times distance per unit area (i.e. A_θ and $\overline{A}$ have units of m$^{1/2}$) whereas A_{Ix} and A_{Iy} are absolute amplitudes (i.e. units of m). For large enough values of A_{Ix} and A_{Iy}, *SNR* is proportional to $A_\theta^2/(A_{Ix}A_{Iy})$. All other expressions for *SNR* could be modified in a similar fashion by including the extra terms in equation (18) in calculating the 'noise' term.

[63] Finally, we observe that if coherent amplitudes (A_θ and $\overline{A}$) are relatively constant and the primary source of variability in ambient noise levels is in the incoherent amplitudes (A_{Ix}), then equation (62) shows that the *SNR* will be inversely related to total ambient noise level. This result is in good agreement with the results of *Lin et al.* [2006], who show that noise correlation *SNR* is generally higher for quiet stations and lower for high-noise stations. The strong dependence observed by *Lin et al.* [2006] suggests that the incoherent noise amplitudes, A_{Ix}, can often be relatively large compared with the coherent noise amplitudes. The much larger variation in incoherent noise levels may be due to large differences in local anelastic effects such as fluid-flow induced tilt and seafloor deformation [*Lin et al.*, 2006].

3.2.6. Summary of Section 3.2

[64] In sections 3.2.1–3.2.5, we have shown how the signal-to-noise ratio, *SNR*, depends on the assumed noise source distribution (summarized in Table 1, including the reflection case as discussed in Appendix C). We find that the *SNR* generally increases linearly with $\sqrt{c/(\omega r_{xy})}$, $\sqrt{T_0/T_a}$, and the square of the amplitude ratio between coherent and incoherent terms (e.g., $A_\theta^2/\overline{A}^2$). However, the dependence of the *SNR* on r_{xy} depends on the noise source distribution, with no further dependence on r_{xy} in the far-field case (see equation (51)), exponential decay in the uniform case (see equation (56)), and an even faster decay in the near-field case (see equation (60)). These results allow researchers to calculate whether it is likely that a particular deployment of seismometers would potentially yield a robust noise correlation measurement.

4. Conclusion

[65] In section 2, we have described in general terms how the cross correlation depends on the distribution of noise

sources in a ray-theoretical framework. This goes beyond previous work by including the effects of attenuation and therefore this framework can be used to quantify how the amplitudes of cross correlations depend on various parameters. In section 3, we have applied this framework to understand how attenuation measurements can be made from coherency (section 3.1) and to understand how one can infer the signal-to-noise ratio for a given situation (section 3.2). In section 3.1, we have shown that the decay of coherency with station spacing depends crucially on the distribution of noise sources. As a result, in order to make accurate attenuation measurements, one needs to first quantify this distribution. In section 3.2, we have shown that (to first order) the signal-to-noise ratio depends on a small number of parameters that can often be estimated. This allows researchers to potentially estimate the robustness of a noise correlation measurement prior to making the measurement. Beyond the 2 specific accomplishments just listed, the theoretical framework provided can also potentially be used to analyze other features of noise correlation measurements.

Appendix A: Additional Background Noise: Example for Reflection

[66] Since only signals that are generated from within the same attenuation time ($T_a = Q_P/\omega$) add coherently, so far it has been assumed that all of the signals of interest are of this type. However, there are a few important cases where the signal of interest may occur at a time lag for which most sources contribute incoherently, e.g. when the responses are due to sources that differ in time by more than T_a.

[67] Here, we concentrate on perhaps the simplest (and maybe most important) example of a body-wave reflection response (in which case, $D = 1$). In this case, $\boldsymbol{x} \approx \boldsymbol{y}$, and one is interested in a potential signal occurring at time delay $\Delta t = 2\Delta z/c$ where Δz is the layer thickness and c is the average velocity of the layer (see Figure 1f for a schematic). Since $\boldsymbol{x} \approx \boldsymbol{y}$, then $r_{jy} - r_{jx} \approx 0$ so that all primary sources (excluding, e.g., the reflection response) have their cross-correlation response at $t \approx 0$. Now, if $\Delta t \gg T_a$ then at a correlation lag time of Δt all of the primary sources would have their correlations between sources not within the same T_a and therefore would have phases that are independent of each other. Here, we show an example of this for a situation in which there are 2 independent noise sources ($\boldsymbol{s}_1$ and $\boldsymbol{s}_2$) plus a reflection response from source $\boldsymbol{s}_1$ at Δt. Assuming that $\boldsymbol{x} \approx \boldsymbol{y}$, $\Delta t \gg T_a$ and that the delay of interest is Δt then we can write

$$
\begin{aligned}
{}_iu(\boldsymbol{x}, t, t_0) \;&= A_1\epsilon(r_{1x})\;\cos\left[\omega\left(t - \frac{r_{1x}}{c}\right) + \phi_{1i}\right] \\
&+ A_2\epsilon(r_{2x})\;\cos\left[\omega\left(t - \frac{r_{2x}}{c}\right) + \phi_{2i}\right] \\
&+ \Gamma A_1\epsilon(r_{1x})\;\cos\left[\omega\left(t - \frac{r_{1x}}{c} - \Delta t\right) + \phi_{3i}\right] \qquad \text{(A1)}
\end{aligned}
$$

$$
\begin{aligned}
{}_iu(\boldsymbol{y}, t, t_0 + \Delta t) \;&= A_1\epsilon(r_{1y})\;\cos\left[\omega\left(t - \frac{r_{1y}}{c}\right) + \phi_{4i}\right] \\
&+ A_2\epsilon(r_{2y})\;\cos\left[\omega\left(t - \frac{r_{2y}}{c}\right) + \phi_{5i}\right] \\
&+ \Gamma A_1\epsilon(r_{1y})\;\cos\left[\omega\left(t - \frac{r_{1y}}{c} - \Delta t\right) + \phi_{1i}\right], \qquad \text{(A2)}
\end{aligned}
$$

where Γ is a reflection coefficient, and ${}_iu(x, t, t_0)$ represents the response at time t within a window centered at time t_0. Importantly, one should note that the ϕ are all different except that ϕ_{1i} is shared between the direct primary source of $\boldsymbol{x}$ and the reflected response of $\boldsymbol{y}$. Taking $\boldsymbol{x} = \boldsymbol{y}$, then the cross correlation response is then given by

$$
\begin{aligned}
2C^E_{xyM} = \;&\Gamma A_1^2\epsilon^2(r_{1x})\;\cos[\omega(t - \Delta t)] \\
&+ \frac{1}{\sqrt{M}}\Big\{A_1^2\epsilon^2(r_{1x})\;\left(\cos\left[\omega t + \phi_1^{av}\right]\;+ \Gamma^2\cos\left[\omega t + \phi_2^{av}\right]\right) \\
&+ A_1A_2\epsilon(r_{1x})\;\epsilon(r_{2x})\;\cos\left[\omega\left(t - \frac{r_{2x} - r_{1x}}{c}\right)\;+ \phi_3^{av}\right] \\
&+ A_2^2\epsilon^2(r_{2x})\;\cos\left[\omega t + \phi_4^{av}\right]\;+ \ldots\Big\}. \qquad \text{(A3)}
\end{aligned}
$$

Appendix B: Approximate Analysis for Azimuthal Variability in A_s

[68] When A_s varies azimuthally (but covers the entire 2D plane), the result of *Snieder* [2007] can no longer be applied directly, and we resort to calculations like the ones of previous sections. However, in contrast to the far-field cases examined before, the assumption of equation (3) is only an approximation for near-field sources. In particular, the term $\cos(x + \pi/4)/\sqrt{x}$ is used to approximate $J_0(x)$. This approximation makes 2 primary errors. First, it ignores a factor of $\sqrt{2/\pi}$ in the asymptotic form of the Bessel function [*Watson*, 1952]. This error is unimportant in previous results since including it would simply multiply all results by a constant factor of $2/\pi$ (and not affect the form of any expressions). The second error, which is also unimportant for far-field sources, is the fact that it makes use of an asymptotic approximation that is only appropriate for $x \gg 1$, so that equation (3) is only really appropriate when $r \gg r_{xy}$. Despite these known problems, we shall proceed to use equation (3) to approximate all sources (including near-field source). We will therefore obtain approximations that can be compared with the exact results of equation (36)–(38) when A_s is constant. Performing this analysis not only gives insight into how expressions like equation (36) arise but also provide approximate results when A_s varies azimuthally.

[69] It is known that the primary contribution to the cross correlation C^E_{xy} is from around the stationary phase points [*Snieder*, 2004], and including a beam whose width depends on $\omega r_{xy}/c$ [see, e.g., *Lin et al.*, 2008]. The angular width of this beam, θ_0, can be determined by setting the time lag range equal to a fraction of a period (here, this fraction is taken as 1/2, for reasons explained later)

$$
\frac{1}{2}\cdot\frac{2\pi}{\omega} = \frac{r_{xy}\;[1 - \cos(\theta_0/2)]}{c}, \qquad \text{(B1)}
$$

so that θ_0 is given by

$$
\theta_0 = 2\cos^{-1}\left[1 - \frac{\pi c}{\omega r_{xy}}\right]\;\approx 2\cdot\sqrt{\frac{2\pi c}{\omega r_{xy}}}. \qquad \text{(B2)}
$$

An approximation for the cross correlation C^E_{xy} can then be made by assuming that only sources from within this tri-

angular beam of angular size θ_0 contributes significantly to C^E_{xy} (see Figure 1d). If we further assume that $\theta_0 \lesssim 1$ so that $r_{sy} \approx r_{sx} + r_{xy}$ (for positive time lag), and that $A_s \equiv A_\theta$ is constant within this beam (which depends on the azimuth of the station-station direction), then one can integrate over sources in polar coordinates giving

$$2|C^E_{xy}| \approx A_\theta^2 \theta_0 \int_{r_{xy}/2}^{\infty} \frac{e^{-2\alpha r} r}{\sqrt{r^2 - r_{xy}^2/4}} dr = A_\theta^2 \theta_0 \cdot r_{xy} K_1(\alpha r_{xy})/2, \quad \text{(B3)}$$

where $K_k(x)$ is a modified Bessel function of the second kind, of order k. It is worth noting that as $x \to 0$, $xK_1(x) \to 1$, and as $x \to \infty$, $xK_1(x) \to \sqrt{\pi x/2} \cdot e^{-x}$. The decay of amplitude with increasing r_{xy} (and constant θ_0) can be understood as being due to the decrease in the number of sources close to the midpoint of the station-station pair contributing to the cross correlation response. The phasing of C^E_{xy} is not yet determined, but will be discussed below.

[70] On the other hand, the autocorrelation C^E_{xx} does not have this beamed sensitivity, but is instead equally sensitive to noise sources in all directions. Assuming that both stations x and y see approximately the same azimuthal variation and that the average value of A_s^2 is given by $\overline{A}^2$, then again the integral is straightforward and results in

$$2C^E_{xx} \approx \cos(\omega t) \int_0^{\infty} \frac{\overline{A}^2 e^{-2\alpha r}}{r} 2\pi r dr = \frac{\pi \overline{A}^2 \cos(\omega t)}{\alpha}, \quad \text{(B4)}$$

and the same for C^E_{yy}.

[71] The amplitude part of the coherency can now be given by

$$|\hat{C}^E_{xy}| \approx \alpha r_{xy} K_1(\alpha r_{xy}) \frac{A_\theta^2}{\overline{A}^2} \frac{\theta_0}{2\pi} = \alpha r_{xy} K_1(\alpha r_{xy}) \frac{A_\theta^2}{\overline{A}^2} \sqrt{\frac{2c}{\pi \omega r_{xy}}}. \quad \text{(B5)}$$

Observing that equation (B5) should have a Bessel function dependence, as in equation (25), and that the asymptotic form of the Bessel function is $J_0(x) \to \sqrt{2/\pi x} \cdot \cos(x - \pi/4)$, we find that the fraction constant (1/2) chosen above is consistent with the decay of the Bessel function so that we can introduce the phase of C^E_{xy} and $\hat{C}^E_{xy}$ simply by replacing $\sqrt{2/\pi x}$ by $\cos(\omega t) J_0(x)$. Performing this replacement results in

$$2C^E_{xy} \approx \pi A_\theta^2 r_{xy} K_1(\alpha r_{xy}) \cos(\omega t) J_0\left(\frac{\omega r_{xy}}{c}\right) \quad \text{(B6)}$$

$$\hat{C}^E_{xy} \approx \alpha r_{xy} K_1(\alpha r_{xy}) \frac{A_\theta^2}{\overline{A}^2} J_0\left(\frac{\omega r_{xy}}{c}\right). \quad \text{(B7)}$$

[72] We observe that equations (B6) and (B7) closely resemble equations (36) and (38) when $A_\theta = \overline{A}$, i.e. when there is a uniform source distribution (with one of the primary differences being the factor of $2/\pi$ as discussed earlier). Thus, the approximations of equations (B6) and (B7) are not grossly inaccurate. Moreover, they can be easily improved by simply making the substitution $\alpha r_{xy} K_1(\alpha r_{xy}) \to e^{-\alpha r_{xy}}$ and accounting for the $2/\pi$ factor. Making these modifications yields

$$2C^E_{xy} = \frac{2A_\theta^2}{\alpha} e^{-\alpha r_{xy}} \cos(\omega t) J_0\left(\frac{\omega r_{xy}}{c}\right) \quad \text{(B8)}$$

$$\hat{C}^E_{xy} = \frac{A_\theta^2}{\overline{A}^2} e^{-\alpha r_{xy}} J_0\left(\frac{\omega r_{xy}}{c}\right). \quad \text{(B9)}$$

Appendix C: Reflection Signal-to-Noise Ratio

[73] The signal-to-noise ratio can also be determined for the body-wave reflection case as described in Appendix A (see Figure 1f), with C^E_{xyM} given by equation (A3). Before continuing, we remind the reader that this analysis only holds when $\Delta t \gg T_a$. Setting $A_j^* \equiv A_j \epsilon(r_{jx})$ then

$$SNR = \frac{\Gamma A_1^{*2}}{A_1^{*2} + \Gamma^2 A_1^{*2} + 2A_1^* A_2^* + A_2^{*2} + \Gamma(\ldots)} \sqrt{\frac{T_0}{T_a}}. \quad \text{(C1)}$$

One should note that Γ includes any losses along the 2-way reflection path (including potentially an additional reflection at the free surface), and that in most cases of interest $\Gamma \ll 1$. Making the assumption $\Gamma \ll 1$ then the requirement on Γ to retrieve the reflection response is that

$$\Gamma \gtrsim \left[1 + \frac{2A_2^*}{A_1^*} + \frac{A_2^{*2}}{A_1^{*2}}\right] \sqrt{\frac{T_a}{T_0}}. \quad \text{(C2)}$$

On the Earth, A_1 may be thought of as either a far-field body-wave term [e.g., *Gerstoft et al.*, 2008] or a very near-station source (e.g., an oscillator very close to the station), and A_2 may be thought of as the dominant surface-wave noise source term (see Figure 1f). In this case, then $A_2 \gg A_1$. As a perhaps realistic example of retrieving a reflection response from far-field body waves, we take $T_\omega = 5$ s, $T_a \approx 50$ s, $T_0 \approx 1$ yr, and $A_2 \approx 5A_1$. With these assumptions, then we must have $\Gamma \gtrsim 0.03$, i.e. a net reflection coefficient of 3%. Absolute reflection coefficients for reflectors of interest (e.g. the Moho or other crustal reflectors) may be as high as 10% or more [*Warner*, 1990], which suggests that with long correlation times, it may be possible to retrieve reflection responses even when local noise sources are weak [*Zhan et al.*, 2010]. However, in this case, the assumption $\Delta t \gg T_a$ may not be satisfied and so the previous calculation may underestimate the necessary Γ. Although we do not explicitly discuss coda correlations, we note that reflections may be more easily obtained using coda correlations [*Tonegawa et al.*, 2009] compared with ambient noise due to differences in effective noise source distributions.

[74] **Acknowledgments.** The author thanks R. Snieder, F.-C. Lin, G. A. Prieto, M. P. Moschetti, L. Ramirez, D. E. McNamara, two anonymous reviewers and the Associate Editor for helpful comments. This research was supported by a Mendenhall postdoctoral fellowship from the U.S. Geological Survey.

References

Aki, K. (1957), Space and time spectra of stationary stochastic waves, with special reference to microtremors, *Bull. Earthquake Res. Inst.*, *35*, 415–457.

Berger, J., P. Davis, and G. Ekström (2004), Ambient Earth noise: A survey of the Global Seismographic Network, *J. Geophys. Res.*, *109*, B11307, doi:10.1029/2004JB003408.

Brenguier, F., M. Campillo, C. Hadziioannou, N. M. Shapiro, R. M. Nadeau, and E. Larose (2008), Postseismic relaxation along the San Andreas Fault at Parkfield from continuous seismological observations, *Science*, *321*, 1478–1481.

Bromirski, P. D., and F. K. Duennebier (2002), The near-coastal microseism spectrum: Spatial and temporal wave climate relationships, *J. Geophys. Res.*, *107*(B8), 2166, doi:10.1029/2001JB000265.

Cho, K. H., R. B. Herrmann, C. J. Ammon, and K. Lee (2007), Imaging the upper crust of the Korean peninsula by surface-wave tomography, *Bull. Seismol. Soc. Am.*, *97*, 198–207.

Cox, H. (1973), Spatial correlation in arbitrary noise fields with application to ambient sea noise, *J. Acoust. Soc. Am.*, *54*, 1289–1301.

Cupillard, P., and Y. Capdeville (2010), On the amplitudes of surface waves obtained by noise correlation and the capability to recover the attenuation: A numerical approach, *Geophys. J. Int.*, *181*, 1687–1700.

Duffy, M. G. (1982), Quadrature over a pyramid or cube of integrands with a singularity at a vertex, *SIAM J. Numer. Anal.*, *19*, 1260–1262.

Gerstoft, P., P. M. Shearer, N. Harmon, and J. Zhang (2008), Global P, PP, PKP wave microseisms observed from distant storms, *Geophys. Res. Lett.*, *35*, L23306, doi:10.1029/2008GL036111.

Harmon, N., C. Rychert, and P. Gerstoft (2010), Distribution of noise sources for seismic interferometry, *Geophys. J. Int.*, *183*, 1470–1484.

Iri, M., S. Moriguti, and Y. Takasawa (1987), On a certain quadrature formula, *J. Comput. Appl. Math.*, *17*, 3–20.

Larose, E., P. Roux, and M. Campillo (2007), Reconstruction of Rayleigh-Lamb dispersion spectrum based on noise obtained from an air-jet forcing, *J. Acoust. Soc. Am.*, *122*, 3437–3444.

Lin, F.-C., M. H. Ritzwoller, and N. M. Shapiro (2006), Is ambient noise tomography across ocean basins possible?, *Geophys. Res. Lett.*, *33*, L14304, doi:10.1029/2006GL026610.

Lin, F.-C., M. P. Moschetti, and M. H. Ritzwoller (2008), Surface wave tomography of the western United States from ambient seismic noise: Rayleigh and Love wave phase velocity maps, *Geophys. J. Int.*, *173*, doi:10.1111/j1365-246X.2008.03720.x.

McNamara, D. E., and R. P. Buland (2004), Ambient noise levels in the continental United States, *Bull. Seismol. Soc. Am.*, *94*, 1517–1527.

Meier, U., N. M. Shapiro, and F. Brenguier (2010), Detecting seasonal variations in seismic velocities within Los Angeles basin from correlations of ambient seismic noise, *Geophys. J. Int.*, *181*, 985–996, doi:10.1111/j.1365-246X.2010.04550.x.

Mitchell, B. J. (1995), Anelastic structure and evolution of the continental crust and upper mantle from seismic surface wave attenuation, *Rev. Geophys.*, *33*, 441–462.

Prieto, G. A., and G. C. Beroza (2008), Earthquake ground motion prediction using the ambient seismic field, *Geophys. Res. Lett.*, *35*, L14304, doi:10.1029/2008GL034428.

Prieto, G. A., J. F. Lawrence, and G. C. Beroza (2009), Anelastic Earth structure from the coherency of the ambient seismic field, *J. Geophys. Res.*, *114*, B07303, doi:10.1029/2008JB006067.

Roux, P., K. G. Sabra, W. A. Kuperman, and A. Roux (2005), Ambient noise cross correlation in free space: Theoretical approach, *J. Acoust. Soc. Am.*, *117*, 79–84.

Sabra, K. G., P. Gerstoft, P. Roux, W. A. Kuperman, and M. C. Fehler (2005a), Surface wave tomography from microseismcs in Southern California, *Geophys. Res. Lett.*, *32*, L14311, doi:10.1029/2005GL023155.

Sabra, K. G., P. Roux, and W. A. Kuperman (2005b), Emergence rate of the time-domain Green's function from the ambient noise cross-correlation function, *J. Acoust. Soc. Am.*, *118*, 3524–3531.

Sanchez-Sesma, F. J., and M. Campillo (2006), Retrieval of the Green's function from cross correlation: The canonical elastic problem, *Bull. Seismol. Soc. Am.*, *96*, 1182–1191.

Shapiro, N. M., and M. Campillo (2004), Emergence of broadband Rayleigh waves from correlations of the ambient seismic noise, *Geophys. Res. Lett.*, *31*, L07614, doi:10.1029/2004GL019491.

Shapiro, N. M., M. Campillo, L. Stehly, and M. H. Ritzwoller (2005), High-resolution surface-wave tomography from ambient seismic noise, *Science*, *307*, 1615–1618.

Snieder, R. (2004), Extracting the Green's function from the correlation of coda waves: A derivation based on stationary phase, *Phys. Rev. E*, *69*, 1–8.

Snieder, R. (2007), Extracting the Green's function of attenuating heterogeneous acoustic media from uncorrelated waves, *J. Acoust. Soc. Am.*, *121*, 2637–2643.

Tonegawa, T., K. Nishida, T. Watanabe, and K. Shiomi (2009), Seismic interferometry of teleseismic S-wave coda for retrieval of body waves: An application to the Philippine Sea slab underneath the Japanese Islands, *Geophys. J. Int.*, *178*, 1574–1586, doi:10.1111/j.1365-246X.2009.04249.x.

Tromp, J., Y. Luo, S. Hanasoge, and D. Peter (2010), Noise cross-correlation sensitivity kernels, *Geophys. J. Int.*, *183*, 791–819.

Tsai, V. C. (2009), On establishing the accuracy of noise tomography travel-time measurements in a realistic medium, *Geophys. J. Int.*, *178*, 1555–1564, doi:10.1111/j.1365-246X.2009.04239.x.

Tsai, V. C. (2010), The relationship between noise correlation and the Green's function in the presence of degeneracy and the absence of equipartition, *Geophys. J. Int.*, *182*, 1509–1514, doi:10.1111/j.1365-246X.2010.04693.x.

Tsai, V. C., H. Kanamori, and J. Artru (2004), The morning glory wave of southern California, *J. Geophys. Res.*, *109*, B02307, doi:10.1029/2003JB002596.

Warner, M. (1990), Absolute reflection coefficients from deep seismic reflections, *Tectonophysics*, *173*, 15–23.

Watson, G. N. (1952), *A Treatise on the Theory of Bessel Functions*, Cambridge Univ. Press, Cambridge, U. K.

Yao, H., and R. D. van der Hilst (2009), Analysis of ambient noise energy distribution and phase velocity bias in ambient noise tomography, with application to SE Tibet, *Geophys. J. Int.*, *179*, 1113–1132.

Yao, H., R. D. van der Hilst, and M. V. de Hoop (2006), Surface-wave array tomography in SE Tibet from ambient seismic noise and two-station analysis: I. Phase velocity maps, *Geophys. J. Int.*, *166*, 732–744.

Zhan, Z., S. Ni, D. V. Helmberger, and R. W. Clayton (2010), Retrieval of Moho-reflected shear wave arrivals from ambient seismic noise, *Geophys. J. Int.*, *182*, 408–420.

Zurn, W., J. Exss, H. Steffen, C. Kroner, T. Jahr, and M. Westerhaus (2007), On reduction of long-period horizontal seismic noise using local barometric pressure, *Geophys. J. Int.*, *171*, 780–796.

V. C. Tsai, Seismological Laboratory, California Institute of Technology, 1200 E. California Blvd., MS 252-21, Pasadena, CA 91125, USA. (tsai@caltech.edu)